Evaluation of the Effect of Deflection Waveform on Fatigue Test Results for Hot Mix Asphalt

Authors:

Angel Mateos, Rongzong Wu, Erik Denneman,
Angela Liu, and John Harvey

Work Conducted as Part of Partnered Pavement Research Center Strategic Plan Element No. 3.31
(DRISI Task 2668):
Improved Mechanistic-Empirical Design Algorithms and Reliability Approach

PREPARED FOR:

California Department of Transportation
  (Caltrans)
Division of Research, Innovation and System
  Information

PREPARED BY:

University of California
Pavement Research Center
Davis and Berkeley

TECHNICAL REPORT DOCUMENTATION PAGE

1. REPORT NUMBER UCPRC-TM-2015-03	2. GOVERNMENT ASSOCIATION NUMBER	3. RECIPIENT'S CATALOG NUMBER
4. TITLE AND SUBTITLE Evaluation of the Effect of Deflection Waveform on Fatigue Test Results for Hot Mix Asphalt		5. REPORT PUBLICATION DATE November 2017
		6. PERFORMING ORGANIZATION CODE
7. AUTHOR(S) A. Mateos, R. Wu, Erik Denneman, A. Liu, and J. Harvey		8. PERFORMING ORGANIZATION REPORT NO. UCPRC-TM-2015-03
9. PERFORMING ORGANIZATION NAME AND ADDRESS University of California Pavement Research Center Department of Civil and Environmental Engineering, UC Davis 1 Shields Avenue Davis, CA 95616		10. WORK UNIT NUMBER
		11. CONTRACT OR GRANT NUMBER 65A0542
12. SPONSORING AGENCY AND ADDRESS California Department of Transportation Division of Research, Innovation, and System Information P.O. Box 942873 Sacramento, CA 94273-0001		13. TYPE OF REPORT AND PERIOD COVERED Technical Memorandum October 2014 to April 2016
		14. SPONSORING AGENCY CODE

15. SUPPLEMENTAL NOTES

16. ABSTRACT

An experimental study was conducted to determine the effect of deflection waveform on four-point flexural fatigue test results for hot mix asphalt. Seven asphalt mixtures, comprising a wide variety of gradations, binder types, and binder contents, were selected for this study. Four of the mixes were tested at the University of California Pavement Research Center (UCPRC) and three were tested in Australia by the ARRB Group. The mixes were tested at different strain levels under both haversine and sinusoidal deflection-controlled modes without introducing rest periods between load cycles. The haversine and sinusoidal testing modes were compared to each other from different perspectives. This comparison showed no indications of differences in damage as measured by stiffness reduction between the haversine and sinusoidal waveforms for six of the seven mixtures. This outcome was attributed to the viscoelastic nature of asphalt mixes. Because of this viscoelasticity, it is believed that the beam at-rest position in haversine testing will move to halfway between zero and maximum deflection, and so the same stress is produced by haversine and sinusoidal deflection waveforms as soon as the peak-to-peak deflection amplitudes are equal. For one of the seven mixes, sinusoidal testing produced considerably longer fatigue lives. No reason was found to explain why the results for this mix differed considerably from the results with the other mixes. Based on these results, no compelling reason was found to recommend that UCPRC change from its use of a haversine to a sinusoidal mode of testing, but similarly no reason was found not to make this change. One reason to move to the sinusoidal wave is that in terms of stress, haversine testing becomes sinusoidal after a small number of load repetitions. It is therefore recommended that the UCPRC and Caltrans support the standardization of waveform requirements in the ASTM and AASHTO test methods to use the sinusoidal waveform because the same fatigue life and stiffness degradation curves are expected from the two testing modes when rest periods are not included between loading cycles. It is anticipated that none of the historical fatigue model parameters calibrated by UCPRC would need to be adjusted. Also examined in the study was the use of alternative failure criteria compared with the currently used criterion of 50 percent loss of stiffness.

17. KEY WORDS Hot mix asphalt, fatigue testing, sinusoidal loading, haversine loading, mechanistic-empirical design	18. DISTRIBUTION STATEMENT No restrictions. This document is available to the public through the National Technical Information Service, Springfield, VA 22161	
19. SECURITY CLASSIFICATION (of this report) Unclassified	20. NUMBER OF PAGES 58	21. PRICE None

Reproduction of completed page authorized

UCPRC ADDITIONAL INFORMATION

1. DRAFT STAGE Final	2. VERSION NUMBER 1
3. PARTNERED PAVEMENT RESEARCH CENTER STRATEGIC PLAN ELEMENT NUMBER 3.31	4. DRISI TASK NUMBER 2668
5. CALTRANS TECHNICAL LEAD AND REVIEWER(S) Imad Basheer, Kee Foo, Sri Balasubramanian	6. FHWA NUMBER CA182668A

7. PROPOSALS FOR IMPLEMENTATION
Based on the results of this experimental study, it is recommended that the UCPRC and Caltrans support the standardization of use of sinusoidal waveform requirements in the ASTM and AASHTO test methods. This recommendation should be further evaluated if testing considers low temperatures or less viscoelastic mixes. It is also recommended that Caltrans consider changing to a failure criterion in performance-related specifications of $E^*{\times}n$ rather than 50 percent loss of stiffness.

8. RELATED DOCUMENTS

9. LABORATORY ACCREDITATION
The UCPRC laboratory is accredited by AASHTO re:source for the tests listed in this report

10. SIGNATURES

A. Mateos **FIRST AUTHOR**	J.T. Harvey **TECHNICAL REVIEW**	D. Spinner **EDITOR**	J.T. Harvey **PRINCIPAL INVESTIGATOR**	I. Basheer **CALTRANS TECH. LEADS**	T.J. Holland **CALTRANS CONTRACT MANAGER**

Reproduction of completed page authorized

DISCLAIMER

This document is disseminated in the interest of information exchange. The contents of this report reflect the views of the authors who are responsible for the facts and accuracy of the data presented herein. The contents do not necessarily reflect the official views or policies of the State of California or the Federal Highway Administration. This publication does not constitute a standard, specification or regulation. This report does not constitute an endorsement by the Department of any product described herein.

For individuals with sensory disabilities, this document is available in alternate formats. For information, call (916) 654-8899, TTY 711, or write to California Department of Transportation, Division of Research, Innovation and System Information, MS-83, P.O. Box 942873, Sacramento, CA 94273-0001.

ACKNOWLEDGMENTS

PROJECT OBJECTIVES

This study is part of Partnered Pavement Research Center Strategic Plan Element (PPRC SPE) 3.31, which is titled "Improved M-E Design Algorithms and Reliability Approach." The goal of the project is to continue improving the M-E design system developed by UCPRC for California pavement design. One of the specific objectives of SPE 3.31 is evaluation of the effect of two deflection waveforms, namely haversine and sinusoidal waveforms, on four-point flexural beam fatigue (4PFBF) test results. The objective was to be achieved by completion of the following tasks:

- Identify representative asphalt concrete mixes to be used in this study
- Conduct 4PFBF tests on each mix using both deflection waveforms
- Analyze the test results
- Submit a technical memorandum summarizing the results

All of these objectives are completed with the publication of this technical memorandum.

TABLE OF CONTENTS

LIST OF FIGURES

LIST OF TABLES

LIST OF ABBREVIATIONS USED IN THIS TECHNICAL MEMORANDUM

4PFBF	Four-point flexural beam fatigue
AASHTO	American Association of State Highway and Transportation Officials
ASTM	American Society for Testing and Materials
C.I.	Confidence Interval
EME	Enrobé bitumineux à module élevé (high-modulus asphalt concrete)
EN	European Normative
FHWA	Federal Highway Administration
HMA	Hot mix asphalt
HMA-PM	Hot mix asphalt-polymer-modified binder
HMA-RB	Hot mix asphalt-rubber binder
NMAS	Nominal maximum aggregate size
RHMA-G	Rubberized hot mix asphalt-gap-graded
SR	Stiffness ratio
TRB	Transportation Research Board
UCPRC	University of California Pavement Research Center

1   INTRODUCTION

The four-point flexural beam fatigue (4PFBF) test has long been used to evaluate fatigue performance of asphalt concrete at intermediate pavement temperatures *(1)*. This test measures *damage,* defined as the loss of flexural stiffness of an asphalt concrete beam while it is subjected to repeated flexural bending. The beam can be either a laboratory sample or a specimen cut from a field pavement *(2)*.

Current U.S. practice for 4PFBF testing on asphalt concrete follows one of two standard methods: ASTM D7460-10 *(2)* or AASHTO T 321-14 *(3)*. Both of these were developed from research findings made by the SHRP A-003A project *(1)* completed in 1994.

Over the years the ASTM and AASHTO test methods have undergone several rounds of changes, rendering the current versions very similar to each other. However, the way that each specifies how load is to be applied to the beam remains a major difference between them: the ASTM method states that the loading device shall be capable of providing "cyclic haversine loading," while the AASHTO method requires the loading device to be capable of providing "repeated sinusoidal loading."

Since both ASTM and AASHTO methods are run in displacement-controlled mode, the words "haversine" and "sinusoidal" in the loading descriptions refer to the waveforms of the displacements imparted to the beam by the loading device. The cyclic haversine loading is clearly understood as displacement waveform in the shape of a displaced sine wave with full amplitude on one side of zero. The repeated sinusoidal loading on the other hand is less specific because it merely requires the displacement waveform to follow a sine wave, whose general form can be written:

$$y(t) = A \cdot \sin(2\pi f t + \varphi) + D \tag{1}$$

$$\text{where:} \quad t = \text{time}$$
$$A = \text{half of peak-to-peak oscillation,}$$
$$f = \text{loading frequency,}$$
$$\varphi = \text{initial phase angle, and}$$
$$D = \text{center amplitude.}$$

When $\varphi = \frac{\pi}{2}$ and $D = A$, Equation (1) represents the haversine waves required by the ASTM test method. When $\varphi = 0$ and $D = 0$, Equation (1) represents sine waves oscillating around zero that some assume the AASHTO test method requires *(4)*. Technically, the AASHTO test method allows the use of haversine displacement waveforms, among many other possible combinations of initial phase angle and center amplitude. A similar

situation exists with the European standard for 4PFBF, EN 12697-24:2012 Annex D, which specifies that "the applied load shall vary sinusoidally" and "the beam shall be moved sinusoidally" *(5)*. Within European countries this is typically interpreted as a sine wave oscillating around zero *(6)*.

To avoid confusion, in this memorandum a sinusoidal waveform is referred to as a sine wave with zero initial phase angle and zero center amplitude (i.e., $\varphi = 0$ and $D = 0$). An illustration of the two waveforms is shown in Figure 1.1.
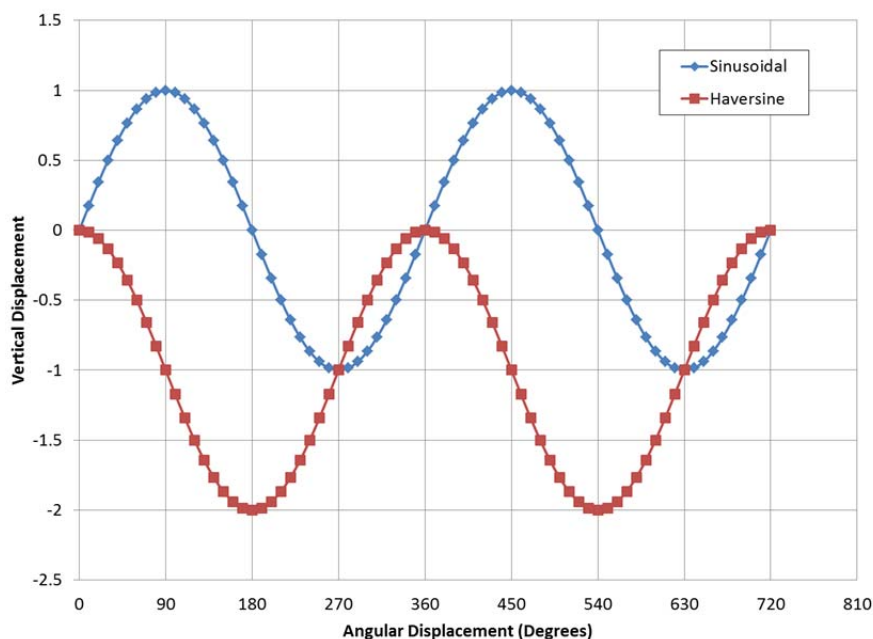
Figure 1.1: Illustration of sinusoidal and haversine waveforms for vertical displacement.
(Note: positive vertical displacement can correspond to either upward or downward movements.)

Although the deflection waveform was not clearly specified in the SHRP A-003A report *(1),* haversine waveforms were used, as the raw data on page 95 of that report show. The University of California Pavement Research Center (UCPRC) has been conducting 4PFBF tests using haversine waveforms since 1991. This has also been the typical practice for most researchers around the world *(4)*. Conceptually a haversine waveform simulates field conditions better than a sinusoidal waveform because the passing of a truck will mainly push a pavement downward.

Some confusion has also been created around the different ways that 4PFBF test standards report strain since the ASTM standard reports the peak-to-peak value while the AASHTO and EN standards are typically run in sinusoidal mode with the reported strain being the zero-to-peak value (half the peak-to-peak strain). This confusion has led some authors to warn that a factor of two must be applied when comparing strain results

obtained with ASTM and EN standards *(6, 7)*. Further examination of the resulting displacement, strain, and stress waveforms during 4PFBF tests led some to conclude *(4)* that 4PFBF tests run with a haversine waveform tend to yield erroneous results since the test assumptions do not match actual test conditions. Their point is that both the haversine and the sinusoidal displacement waveforms produce a sinusoidal load waveform for nearly all of a given test, with the haversine load wave changing to a sinusoidal shape soon after initiation of the test while the load waveform is always sinusoidal when there is a sinusoidal displacement waveform. These authors recommend that ASTM change its standard deflection-controlled waveform to sinusoidal from haversine. So far, however, the arguments against performing haversine 4PFBF tests remain unsupported by actual data. Other authors *(8)* caution against replacing the haversine waveform with the sinusoidal waveform altogether before sufficient substantiating data is obtained. Most of the control software in testing devices used for 4PFBF around the world uses a sinusoidal waveform.

The issues raised by the differences in deflection waveforms specified by the ASTM and AASHTO test methods are the reason that in April 2015 the Federal Highway Administration (FHWA) asphalt mixture expert task group charged an ad hoc committee to standardize the 4PFBF test. After its work the committee did not reach a consensus on a specific displacement waveform. Instead it recommended that both sinusoidal and haversine waveforms could be used, but that the selected waveform must be reported.

Over the years, the UCPRC has accumulated a large amount of 4PFBF test data. These data were collected using haversine waveforms without rest periods. The data capture the laboratory fatigue performance of various asphalt concrete mixes and are critical components of the mechanistic-empirical design method under continual development by the UCPRC for California pavements included in the software *CalME*. Given the ongoing controversies regarding the deflection waveforms to be used in 4PFBF, it is necessary to investigate the correlation between test results produced by the two displacement waveforms. The findings of this investigation will help UCPRC, Caltrans, and others decide whether to keep running 4PFBF tests using a haversine waveform or to change to use of a sinusoidal waveform. The decision will need to be codified into changes in standard practice for 4PFBF testing, either by referencing updated and harmonized AASHTO and ASTM tests, or directly in Caltrans specifications that include 4PFBF testing such as the Caltrans Long-Life Asphalt Pavement (LLAP) specifications.

1.1 Problem Statement

The four-point flexural bending fatigue test is used by researchers and industry to evaluate the fatigue performance of asphaltic concrete mixes. The test has been conducted mainly using haversine waveforms for

displacement control following the ASTM standard test method. The alternative AASHTO test method specifies the use of sinusoidal waveforms. Theoretical considerations recently raised uncertainties about how appropriate it is to use the haversine waveform in 4PFBF testing, and a recommendation was made to exclusively use sinusoidal waveforms for these tests. This recommendation was made despite a lack of data showing that haversine waveform use has actually led to problems.

UCPRC has conducted 4PFBF tests using haversine waveforms for many years. The new concerns raised about use of this waveform are therefore significant because they affect how the large amount of historical data accumulated by UCPRC and the majority of other researchers should be used. UCPRC has used the stiffness degradation curves recorded during 4PFBF to identify the fatigue damage model parameters needed as inputs to the mechanistic-empirical design method included in *CalME*. If there is a difference between results obtained using haversine and sinusoidal waveforms, then a change by Caltrans and the UCPRC to use of the sinusoidal waveform would require a recalibration of the fatigue models. Despite the new concerns raised about use of the haversine waveform, it should be noted that after rigorous evaluation, the SHRP A-003A project *(1)* selected this method of 4PFBF as the best alternative for evaluating asphalt concrete fatigue performance. Therefore it should not be necessary to reinvestigate whether 4PFBF test using haversine waveform provides reasonable results, at least not as a first step.

Because of the concerns regarding the use of haversine waveforms in 4PFBF tests, a decision was made to conduct an experimental study to collect test data using both waveforms for the same set of mixes. The main objective of the study was to investigate the effect of the two displacement waveforms on the results of 4PFBF tests that do not include rest periods between load pulses. By comparing the results generated by testing using the two waveforms, the study aimed to answer the following questions:

- Are results from the haversine and sinusoidal tests similar, if everything else is equal?
- If not, is there a strong correlation between them?

If the answer to either of the above questions is yes, then there is no need to replace the haversine waveform with a sinusoidal waveform when rest periods are not included. A yes answer to both questions also means that a switch to the sinusoidal waveform would not require recalibration of existing models and data. On the other hand, if the answer to both questions is no, a switch to the sinusoidal waveform would require recalibration of existing models.

1.2 Goals, Objectives, and Deliverables

This study is part of Strategic Plan Element (SPE) 3.31, which is titled "Improved M-E Design Algorithms and Reliability Approach." The goal of the project is to continue improving the M-E design system developed by UCPRC for California pavement design. One of the specific objectives of SPE 3.31 is evaluation of the effect of two deflection waveforms—namely, the haversine and sinusoidal waveforms—on 4PFBF test results. The objective was to be achieved by completion of the following tasks:

1. Identify representative asphalt concrete mixes to be used in this study,
2. Conduct 4PFBF tests on each mix using both deflection waveforms,
3. Analyze the test results, and
4. Submit a technical memorandum summarizing the results.

This technical memorandum presents the results from each of these tasks. It should be noted that this research was conducted as part of a pooled effort with the ARRB Group Ltd (ARRB) of Australia without any exchange of financial resources. ARRB conducted independent tests on selected asphalt concrete mixes used in Australia. The test data from both UCPRC and ARRB were pooled for the analysis.

2 EXPERIMENTAL DESIGN

An experimental study was conducted to determine the difference in fatigue test results between two displacement waveforms: haversine and sinusoidal. Seven mixes were selected and tested in both displacement-controlled modes. The results from the two types of loading were then analyzed to detect potential differences, and, if there were any, the reasons for these differences were sought.

2.1 Selection of Representative Asphalt Concrete Mixes

Four asphalt mixes considered to be representative of the variety of mixes used by Caltrans were selected for the study. These mixtures were tested at the UCPRC using a four-point flexural beam fatigue (4PFBF) fatigue testing machine manufactured by Cox & Sons Inc. In addition, three mixes representative of Australian materials were selected and tested by the ARRB Group using an IPC 4PFBF fatigue machine. A brief description of each mix is presented below.

The California mixes:

- RHMA-G is a rubberized gap-graded mix, 19 mm (¾ in.) nominal maximum aggregate size (NMAS), meeting Caltrans Superpave design requirements with 8.8 percent asphalt rubber binder content. The aggregate type is crushed granite and the binder has a PG 64-16 base with minimum 18 percent recycled tire rubber.

- HMA is a conventional dense-graded mix, 19 mm (¾ in.) NMAS, meeting Superpave design requirements with 5.9 percent binder content. The aggregate type is crushed granite and the binder type is PG 70-10.

- HMA-PM is a dense-graded mix, 19 mm (¾ in.) NMAS, meeting Hveem design requirements with a 5.0 percent content of polymer-modified (PM) binder meeting PG 64-28 requirements. The aggregate type is crushed river alluvial.

- HMA-RB meets Caltrans long-life performance-related specifications from a project on I-5 in Tehama County (Northern California) and is a rich-bottom mix, 19 mm (¾ in.) NMAS, with 5.9 percent binder content. The aggregate type is crushed alluvial and the binder type is PG 64-10.

The Australia mixes:

- DG10 C320 is a dense-graded mix, 10 mm (0.4 in.) NMAS, with 5.6 percent binder content. The aggregate type is crushed granite and the binder meets the requirements for Class 320 (viscosity of approximately 320 Pa.s at 60℃). This mix is typically used as a surface layer.

- DG20 C600 is a dense-graded mix, 20 mm (¾ in.) NMAS, with 4.7 percent binder content. The aggregate type is crushed greywacke and the binder meets the requirements for Class 600 (viscosity of approximately 600 Pa.s at 60°C). This mix is typically used as a base layer.

- EME is a dense-graded, 14 mm (0.55 in.) NMAS, high-modulus asphalt mix with 5.6 percent binder content. The aggregate type is crushed greywacke and the binder meets the requirements for 15/25 penetration grade bitumen according to European specification EN 13924. This mix is typically used as a base layer in thick asphalt pavements.

2.2 Tests Conducted

Each of the Caltrans mixes was tested at two different strain levels, targeted to fail at 0.1 to 0.5 million and 0.5 to 1 million repetitions. Each of the Australian mixes was tested at three strain levels, targeting 10^4, 10^5, and 10^6 repetitions to failure. All the fatigue tests were conducted at either 20°C or 30°C and a 10 Hz loading frequency without introducing rest periods between load pulses. At least three replicates were tested for each strain level in each loading mode (haversine and sinusoidal). A summary of the testing conditions is presented in Table 2.1. Peak-to-peak strain in this table was calculated by using the same formulations for both haversine and sinusoidal tests. In both cases, peak-to-peak strain was determined using the peak-to-peak deflection, and peak-to-peak stress was determined using the peak-to-peak load. *Dynamic modulus* is defined as the ratio of peak-to-peak stress to peak-to-peak strain. For the sinusoidal tests, the peak-to-peak strain value was assumed to be equal to twice the zero-to-peak strain.

Table 2.1: Summary of Testing Conditions

Mix ID	Mix Source	Testing Device	Temp.	Freq.	Strain Level[*]	Peak-to-Peak Strain	Replicates Haversine	Replicates Sinusoidal
RHMA-G	California	Cox & Sons	20°C	10 Hz	Low	470 με	3	3
					Med.	580 με	3	3
HMA	California	Cox & Sons	20°C	10 Hz	Low	270 με	3	3
					Med.	315 με	3	3
HMA-PM	California	Cox & Sons	20°C	10 Hz	Low	505 με	3	3
					Med.	655 με	3	3
HMA-RB	California	Cox & Sons	20°C	10 Hz	Low	350 με	3	3
					Med.	430 με	3	3
DG10 C320	Australia	IPC	20°C	10 Hz	Low	200 με	3	3
					Med.	400 με	3	3
					High	800 με	3	3
DG20 C600	Australia	IPC	30°C	10 Hz	Low	480 με	4	3
					Med.	800 με	3	3
					High	950 με	3	3
EME	Australia	IPC	30°C	10 Hz	Low	460 με	3	8
					Med.	600 με	4	6
					High	760 με	3	6

Note: Additional tests were conducted with the DG20 C600 and EME mixtures at strain levels other than those reflected in the table. Results from these other tests were used in the study to estimate fatigue law parameters.

[*]: The designation of "strain level" is specific to each mix.

Fatigue tests conducted at the UCPRC were continued until beam stiffness diminished to 20 percent of the initial value so that complete failure of the specimen was ensured. Fatigue tests conducted at ARRB were continued until the 50 percent stiffness reduction failure criterion was reached. In all cases, the initial stiffness was determined at 50 load cycles, as specified in the ASTM D7460-10 and AASHTO T 321-14 standards. Three different failure criteria were applied to the data to determine the number of repetitions to failure.

2.3 Analysis Approach

The first step in comparing the effect of sinusoidal versus haversine testing modes was to perform an analysis of the stiffness degradation curves. These curves were analyzed to determine the following parameters: (i) initial dynamic modulus and phase angle, and (ii) number of cycles to failure. Three failure criteria were used: (i) 50 percent stiffness reduction (classical approach), (ii) 60 percent stiffness reduction, and (iii) maximum stiffness multiplied by the number of cycles ($|E^*| \times n$) when plotted versus number of cycles, n. The $|E^*| \times n$ approach is a simplified energy ratio criterion proposed by Rowe and Bouldin *(9)* that has been adopted by both the ASTM D7460-10 and AASHTO T 321-14 standards. The sinusoidal versus haversine testing modes were compared to each other from different perspectives, according to the following steps:

1. Determination of classical fatigue laws. The classical power fatigue laws ($N_f = k_1 \cdot \varepsilon^{-k_2}$) were determined for each mix on the basis of haversine and sinusoidal fatigue lives. Comparison of haversine and

sinusoidal fatigue laws to each other, and their corresponding parameters, provides a first insight into potential differences between the two displacement modes of testing.

2. Analysis of variance (ANOVA) for each individual mix. An ANOVA analysis was conducted on the basis of the results of each specific mix independent of the rest of the mixes. The dependent variable was the number of cycles to 50 percent stiffness reduction. This is the only fatigue life that could be determined for all mixes without extrapolation, since the Australian tests were not continued beyond 50 percent stiffness reduction. Two independent variables were included in this analysis, strain level and test mode (haversine and sinusoidal). The goal of this analysis was to determine the significance level of the test mode factor, and potential interactions between this factor and strain level.

3. Analysis of the shape of the stiffness degradation curves. Average stiffness degradation curves were determined for the tests conducted at medium strain levels (Table 2.1). Two average curves were determined for each mix: one for the haversine replicates and the other for the sinusoidal replicates. Potential differences between the haversine and sinusoidal test modes might not only impact the number of cycles to failure, but also the shape of the stiffness degradation curve. Sinusoidal and haversine average curves determined for each mix were compared visually.

4. Analysis of test results in the Black space. Black diagrams represent dynamic modulus versus phase angle evolution during fatigue testing. These curves have revealed some fatigue phenomena that were not apparent in the stiffness degradation curves *(10)*. For each mix, a set of Black diagrams was plotted for tests conducted in haversine mode and another set for tests conducted in sinusoidal mode. Both sets were compared visually.

5. Analysis of variance for all mixes. An ANOVA analysis was conducted where three factors were included: mix type, test mode, and strain level. The dependent variable was the number of cycles to failure (this time including results obtained for the three failure criteria). Analysis corresponding to 60 percent stiffness reduction and maximum of $|E^*| \times n$ failure criteria could be conducted for mixes tested at the UCPRC and also for one of the Australian mixes whose stiffness reduction curves could be extrapolated beyond the 50 percent stiffness reduction point. The goal of this ANOVA analysis was to determine the significance level of the test mode factor, and the potential interactions between this factor and either strain level or mix type.

3 DATA ANALYSIS

3.1 Analysis of Stiffness Degradation Curves

Complex modulus (E*) degradation curves were analyzed in order to determine several characteristic parameters. First, initial dynamic modulus ($|E^*|$) and phase angle (φ) were determined at 50 load cycles, as suggested by ASTM D7460-10 and AASHTO T 321-14. The initial dynamic modulus, $|E^*|_{INI}$, was first used to calculate the stiffness ratio (SR) for each test cycle (SR = $|E^*|/|E^*|_{INI}$). Then, the number of cycles to failure was determined for the three different failure criteria which were 50 percent and 60 percent stiffness reduction and a maximum of $|E^*| \times n$. In most tests, the number of cycles to failure could be easily determined from the stiffness degradation curves by using simple *Excel* search formulas. In other cases, curve fitting was required to determine the fatigue life according to one or more of the failure criteria. The reasons for conducting curve fitting included the need to interpolate between two loading cycles, to determine the maximum of the curve $|E^*| \times n$ versus number of cycles when it was not clearly seen from the data, to screen out noisy data (only one test), and to extrapolate SR to determine fatigue life beyond 50 percent stiffness reduction for those tests that were stopped there. It should be noted that only short-range extrapolations were conducted, like the example shown in Figure 3.1 below, where the evolution of stiffness versus number of cycles up to the failure point could be inferred from the stiffness measured in previous cycles. In all the ANOVA analyses presented below, it is clearly indicated when extrapolated fatigue lives are used in the analysis. A summary of the test parameters determined in this phase of the analysis is presented in Appendix A.

The curve fitting shown in Figure 3.1 is based on the logit model *(11)*. This model has been shown to reproduce the complete stiffness reduction, up to phase III, by using four independent parameters that can be easily determined with the *Excel* Solver utility. Phase I is the initial rapid loss of stiffness primarily due to internal heating and reversal of thixotropy, phase II is steady state stiffness reduction caused by damage leading to microcracking, and phase III of the stiffness degradation curve is characterized by a sharp decrease of beam stiffness that is typically attributed to microcracks coalescing to form a sharp crack *(9,10)*. This approach was preferred to using splines or polynomials, as recommended by the ASTM and AASHTO 4PFBF standards, because it is both easy and repeatable.
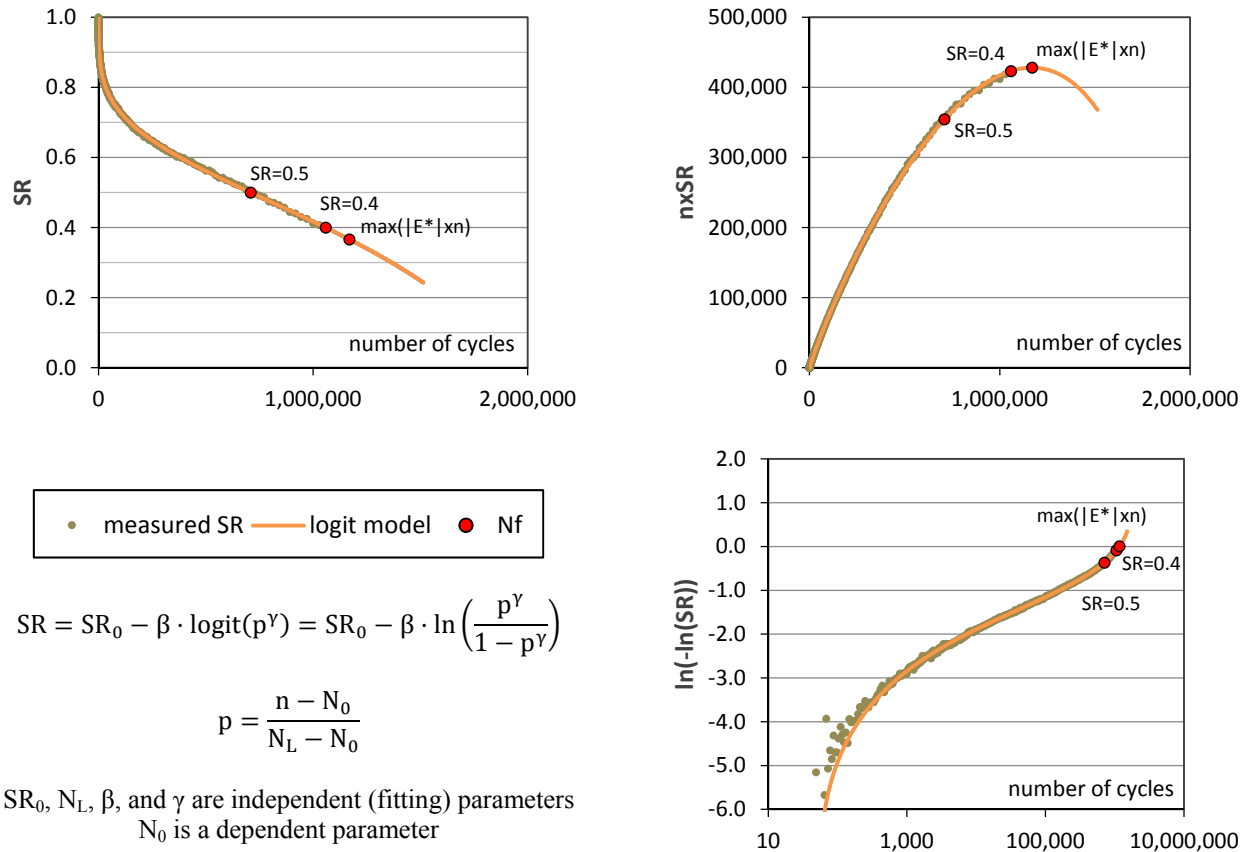
Figure 3.1: Curve fitting to extrapolate fatigue life (HMA-RB, specimen 9S, 350 με peak to peak).

The equations shown in the figure:

$$SR = SR_0 - \beta \cdot logit(p^\gamma) = SR_0 - \beta \cdot \ln\left(\frac{p^\gamma}{1 - p^\gamma}\right)$$

$$p = \frac{n - N_0}{N_L - N_0}$$

SR_0, N_L, β, and γ are independent (fitting) parameters
N_0 is a dependent parameter

3.2 Analysis of Classical Fatigue Laws

A classical fatigue law (Wöhler curve) was fitted to the test results of each mix. The only failure criterion that could be quantified for all the mixes was the one corresponding to 50 percent stiffness reduction. As noted above, the Australia mixes were tested up to 50 percent stiffness reduction, so the maximum value of $|E^*| \times n$ was not typically reached during the tests. This maximum could be extrapolated for most of the tests conducted on the DG10 C320 mix since this failure point was only slightly beyond the 50 percent stiffness reduction cycle, as shown in the example in Figure 3.2. For the same reason, the 60 percent stiffness reduction point (SR=0.4) could be also extrapolated for this mix. However, extrapolation was not regarded as reliable for the other two Australia mixes, so only the fatigue law corresponding to 50 percent stiffness reduction could be determined for them. The same happened for RHMA-G, one of the four Californian mixes, where half of the tests ended before reaching the maximum value of $|E^*| \times n$.

Results of the classical fatigue analysis did not reveal any difference between haversine and sinusoidal fatigue lives for six of the seven mixes included in this study. For these six mixes, the haversine and sinusoidal fatigue

lives seemed to follow the same pattern, as shown in the examples in Figure 3.3 and Figure 3.4. Clear differences were observed for the DG20 C600 mix, however, as Figure 3.5 shows. For this mix, sinusoidal mode testing resulted in a longer fatigue life than haversine mode testing: approximately one to two times longer.
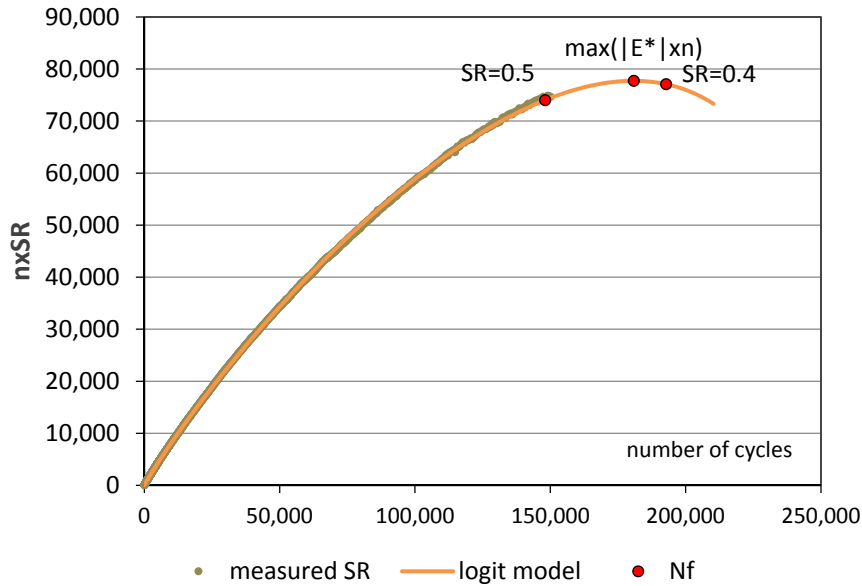
Figure 3.2: Extrapolation of fatigue life (DG10 C320, specimen S2B4H, 400 με peak to peak).
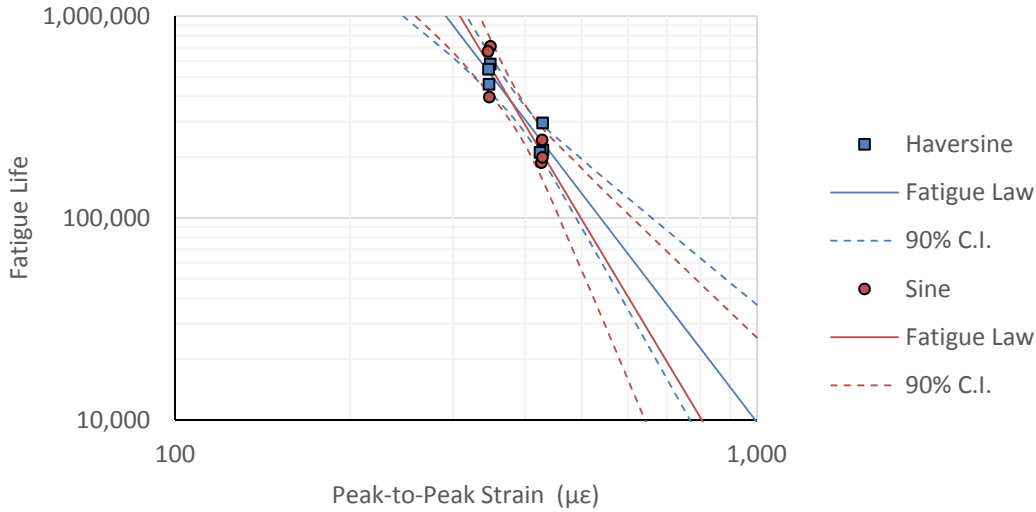
Figure 3.3: Example of classical fatigue laws (HMA-RB, 50% stiffness reduction failure criterion).
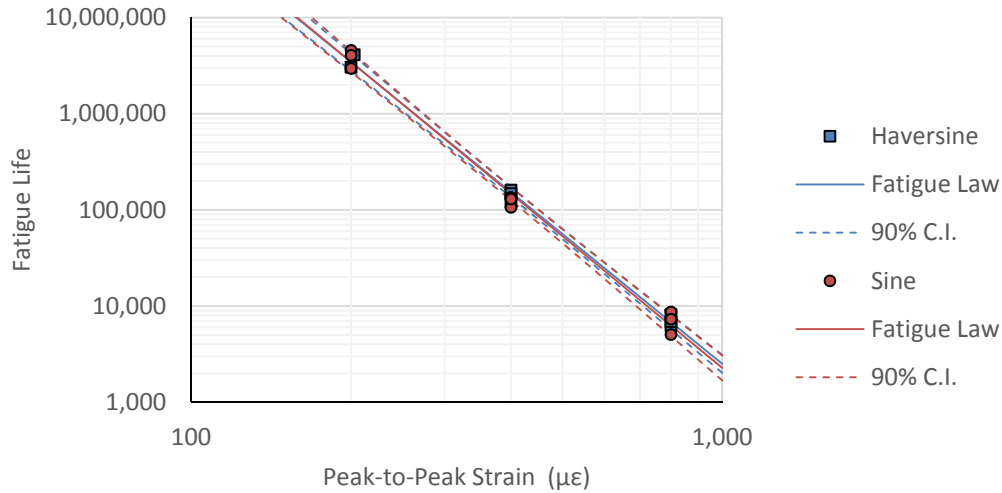
Figure 3.4: Example of fatigue laws (DG10 C320, 50% stiffness reduction failure criterion).
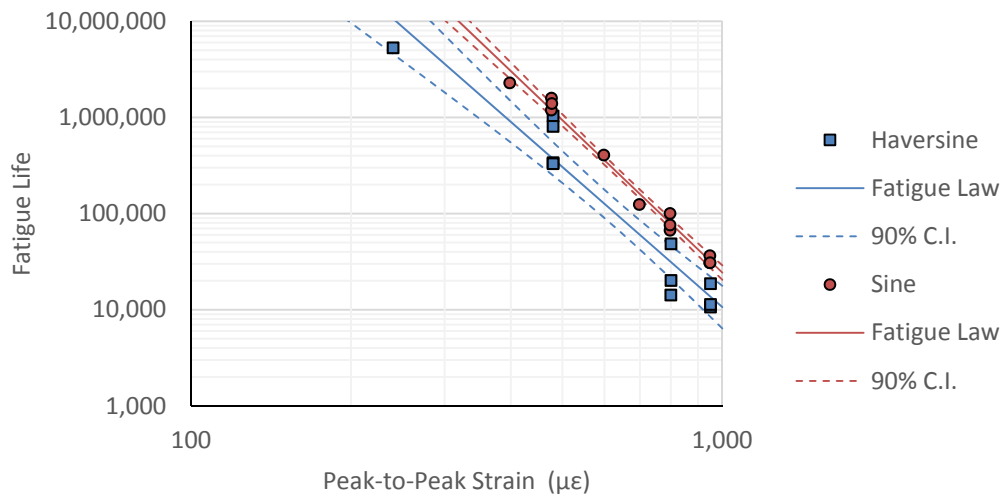
Figure 3.5: Fatigue laws for mix DG20 C600 (50% stiffness reduction failure criterion).
(Note: haversine and sine fatigue lives appeared to differ from each other for this particular mix. [C.I. indicates confidence interval.])

A comparative analysis was also conducted in terms of two main parameters defining the fatigue law of each mix: ε_6 (strain corresponding to a fatigue life of 10^6 cycles) and the slope of the classical fatigue relation. The 50 percent stiffness reduction failure criterion was considered first since this criterion could be determined in all of the tests. Confidence intervals (C.I.) determined for the ε_6 strain for the haversine and sinusoidal test modes overlap for six of the seven mixes, as reflected in Figure 3.6 and Table 3.1. Again, the DG20 C600 mix was the exception. For the slope, similar values were obtained for the haversine and sinusoidal test modes in all the mixes, including DG20 C600 (Figure 3.7). This indicates that for this specific mix the testing mode effect may

reflect a shift in the fatigue law in the double logarithmic scale (log Nf versus log strain). The standard error of the model predictions varied considerably from one mix to another. Nevertheless, similar errors were obtained for the haversine and sinusoidal data in six of the seven mixes. Again, mix DG20 C600 differed from the others, with the errors for haversine and sinusoidal testing being considerably different from each other (Figure 3.8).

The comparative analysis was also conducted on the basis of fatigue lives corresponding to a second failure criterion: the maximum of $|E^*| \times n$ when plotted versus number of cycles. This comparison could be conducted for four of the seven mixtures, and DG20 C600 was not among them. The conclusions support earlier observations since similar ε_6 (see Figure 3.9), slopes, and fitting errors were obtained for the haversine and sinusoidal testing modes. As explained above, this comparison could not be done for mix DG20 C600 since fatigue tests were conducted until a 50 percent stiffness reduction was reached and a reliable extrapolation of the new failure point could not be achieved.
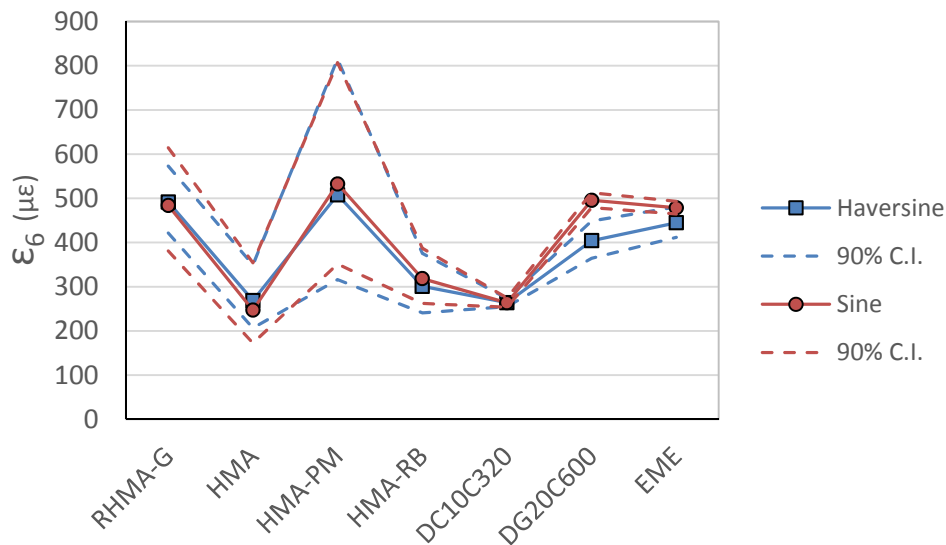
Figure 3.6: Strain (peak-to-peak) corresponding to a fatigue life of 10^6 cycles (50% stiffness reduction failure criterion).
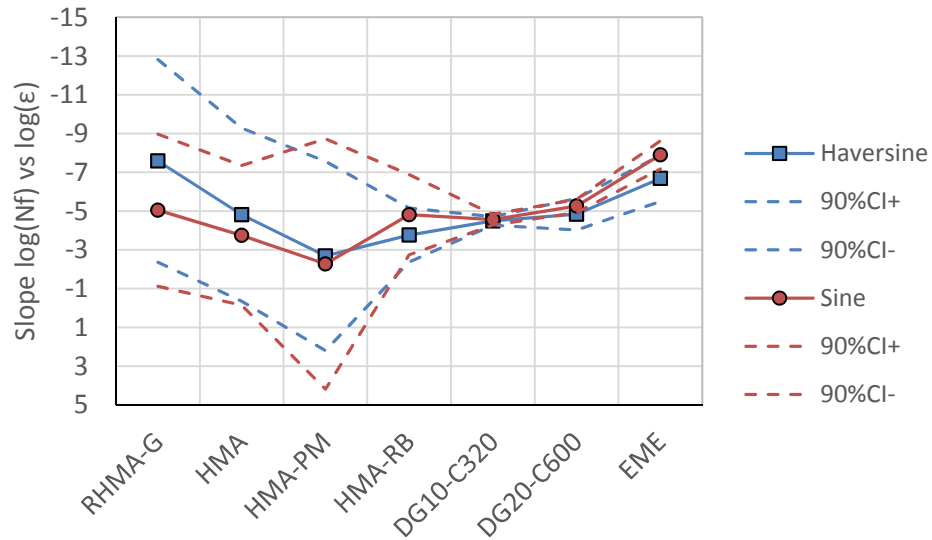
Figure 3.7: Slope of the fatigue law, log(Nf) versus log(ε) (50% stiffness reduction failure criterion). *(Note:* **None of the differences shown in the figure were statistically significant at a 5% significance level. The relatively wide confidence intervals obtained for the Californian mixes are due to the fact that only two strain levels were tested and the two were relatively close.)**
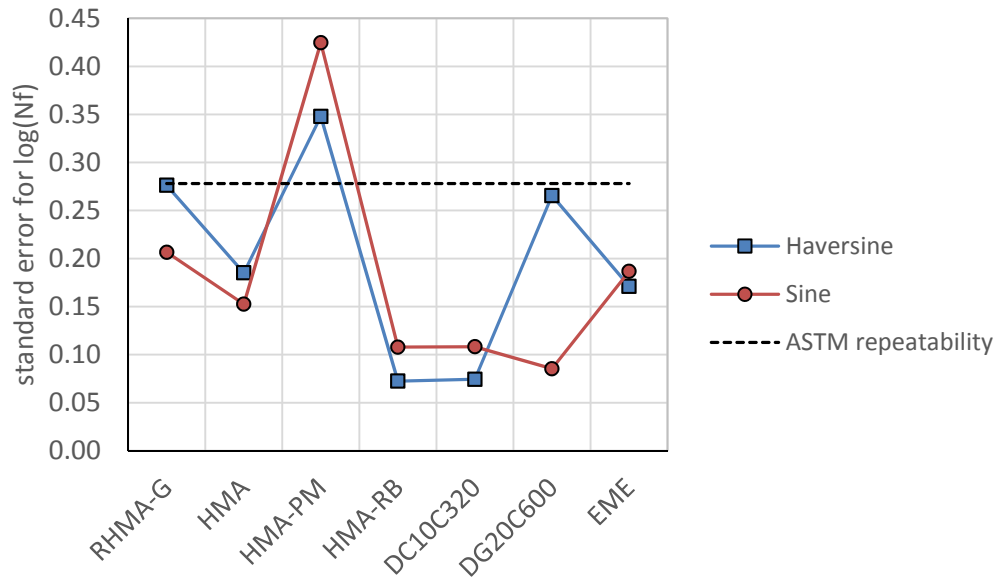
Figure 3.8: Standard error of the fitting, log(Nf) versus log(ε) (50% stiffness reduction failure criterion). (Note: according to ASTM D7460-10, the repeatability standard deviation (in terms of fatigue life) is 0.278 on the log scale. This concept is slightly different from the standard error of the fatigue model shown for each mix in the plot.)

Table 3.1: Confidence Intervals for ε_6 (50% Stiffness Reduction Failure Criterion)

Mix Type	Displacement Mode	ε_6 ($\mu\varepsilon$)		
		90%C.I.-	mean	90%C.I.+
RHMA-G	haversine	422	491	573
	sinusoidal	381	484	615
HMA	haversine	207	269	349
	sinusoidal	172	247	354
HMA-PM	haversine	316	508	815
	sinusoidal	351	532	807
HMA-RB	haversine	241	301	375
	sinusoidal	262	318	387
DG10 C320	haversine	255	264	273
	sinusoidal	253	264	274
DG20 C600	haversine	364	404	449
	sinusoidal	479	496	513
EME	haversine	412	445	480
	sinusoidal	465	479	493

Note: Confidence intervals do not overlap for the DG20 C600 mix (shaded cells).
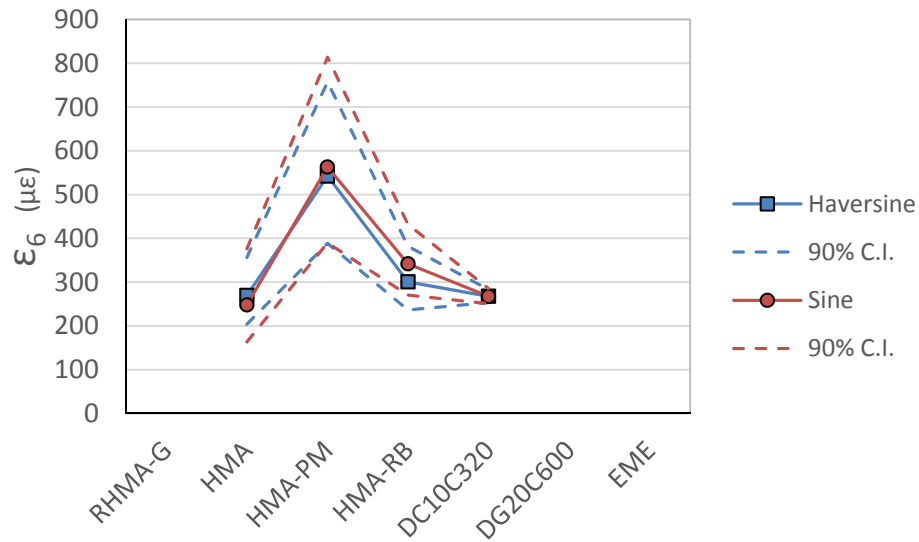
Figure 3.9: Strain (peak-to-peak) corresponding to a fatigue life of 10^6 cycles (max |E*|×n failure criterion). (Note: the DG10 C320 results are based on extrapolated fatigue lives.)

3.3 ANOVA Analysis for Single Mixes

An analysis of variance was conducted for each mix, independent of the other mixes. The study variable was the number of cycles to 50 percent stiffness reduction, which was the only fatigue life that could be determined for all the mixes. Two factors are considered in this ANOVA: strain level and test mode. The factor "strain level" has two possible values for the mixes tested at the UCPRC (low and medium) and three for the mixes tested at ARRB (low, medium, and high), as reflected in Table 2.1. Similarly, the factor "test mode" has two possible

values: haversine or sinusoidal. Both strain level and test mode are fixed factors. Details of this ANOVA analysis are included in Appendix B, which is the output of the statistical software *SPSS*, and a summary with the factors' significance levels is presented in Figure 3.10. The test mode effect was only significant (p-value < 0.05) for the DG20 C600 mix. The interaction between test mode and strain was not significant in any of the cases. This means that the test mode (haversine versus sinusoidal) effect in DG20 C600 mix did not differ from one strain level to another. This result is in line with the earlier observation that haversine and sinusoidal fatigue laws for this mix seem to be parallel to each other.
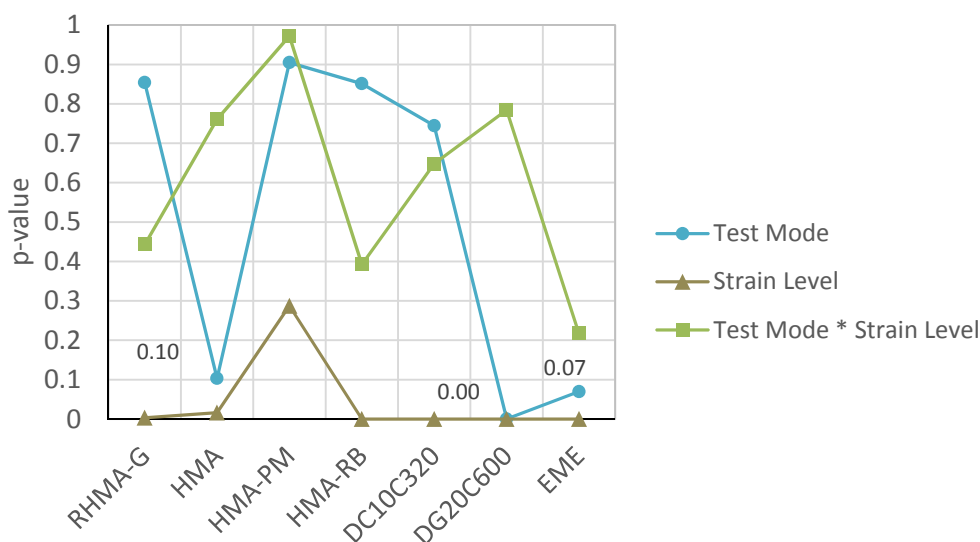
Figure 3.10: ANOVA analysis of single mixes─summary of factors' significance level (study variable is number of cycles to 50% stiffness reduction).

3.4 Analysis of the Shape of the Stiffness Degradation Curves

The stiffness degradation curves were fitted for all the fatigue tests conducted at medium strain level (Table 2.1). The logit model, shown in Figure 3.2 and which has four independent parameters, was used as a fitting function when the tests did not include post failure data.

The logit model, however, cannot reproduce the decreasing rate of damage accumulation in phase III in displacement-controlled fatigue tests (post-failure phase). This decreased damage rate is probably related to a stress-intensity reduction at the crack tips as the applied force lessens in a displacement-controlled test. When tests extended beyond phase III, a modified version of the logit model, termed *logit-logistic,* was used in the fitting process. Figure 3.11 shows an example of this fitting, and details of both the logit and logit-logistic functions can be found in Reference *(11)*. As noted above, the fitting process was conducted for all the medium

strain level tests. In order to define a unique stiffness reduction curve representative of each mix and testing mode, the fitted functions were averaged (average of all replicates for medium strain level). Then the average haversine and sine stiffness degradation curves were scaled (in the cycles axis) so that both resulted in 50 percent stiffness reduction for the same number of cycles. This latter step was taken to make it easier to observe differences in damage (and reversible phenomena) accumulation during the tests. The resulting functions are presented in three different formats in Figure 3.12.

The figure shows that for six of the seven mixes the haversine and sine stiffness degradation curves are almost identical. Some differences for the HMA-RB and HMA-PM mixes appear in phase III, and it is suspected that the differences are related both to the random nature of the macrocracking process and the fact that only three replicates were tested for each mix and testing mode. As before, a different pattern was observed for mix DG20 C600, where the haversine and sine stiffness degradation curves clearly differed from each other. But, contrary to expectation, stiffness reduction at the beginning (phase I) of sine mode testing exceeded that at the beginning of haversine mode testing. The opposite outcome would have been expected since the haversine mode testing results in higher tensile stresses than the sinusoidal mode testing, for the same peak-to-peak strain, during the first cycles of fatigue tests *(6)*.

$$SR = \widehat{SR} \cdot \left[a + \frac{1 - a}{1 + e^{b\left(\frac{n}{N1} - 1\right)}} \right]$$

$\widehat{SR}$ is the logit model, as reflected in Figure 3.2

a, b, and N1 are independent (fitting) parameters
of the sigmoidal part of the model
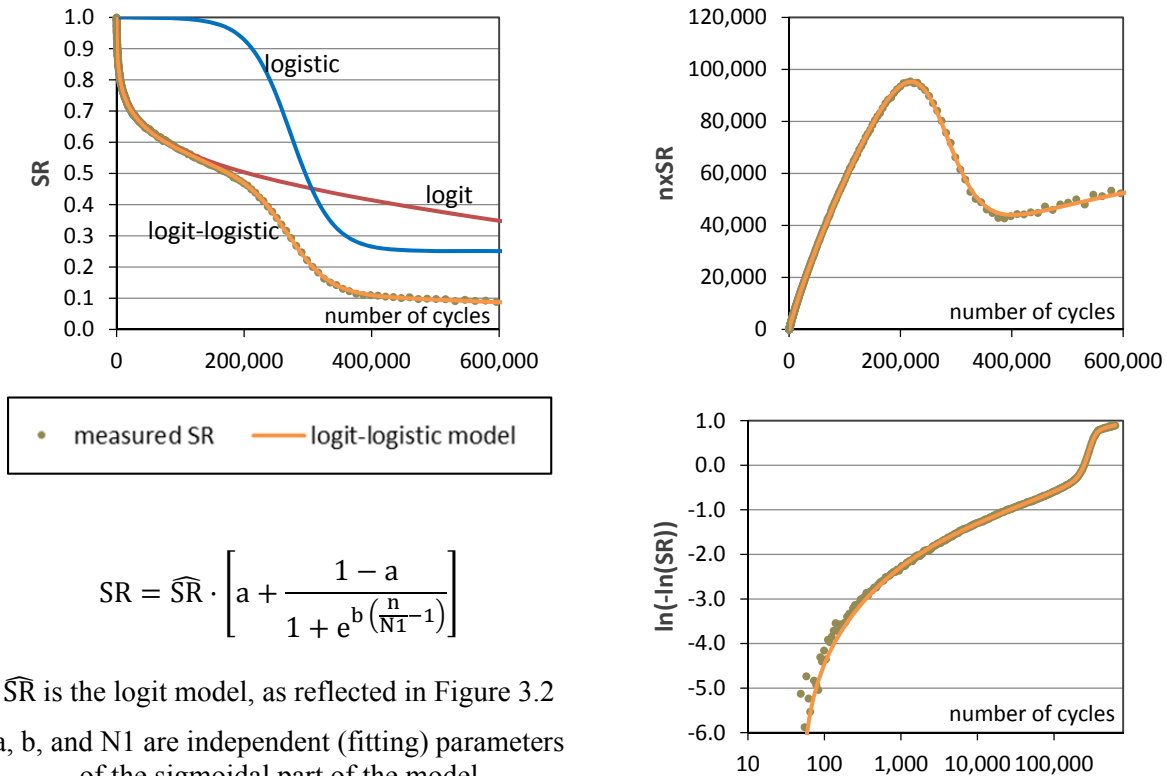
Figure 3.11: Curve fitting beyond failure (RHMA-G, specimen 41H, 580 με peak to peak).
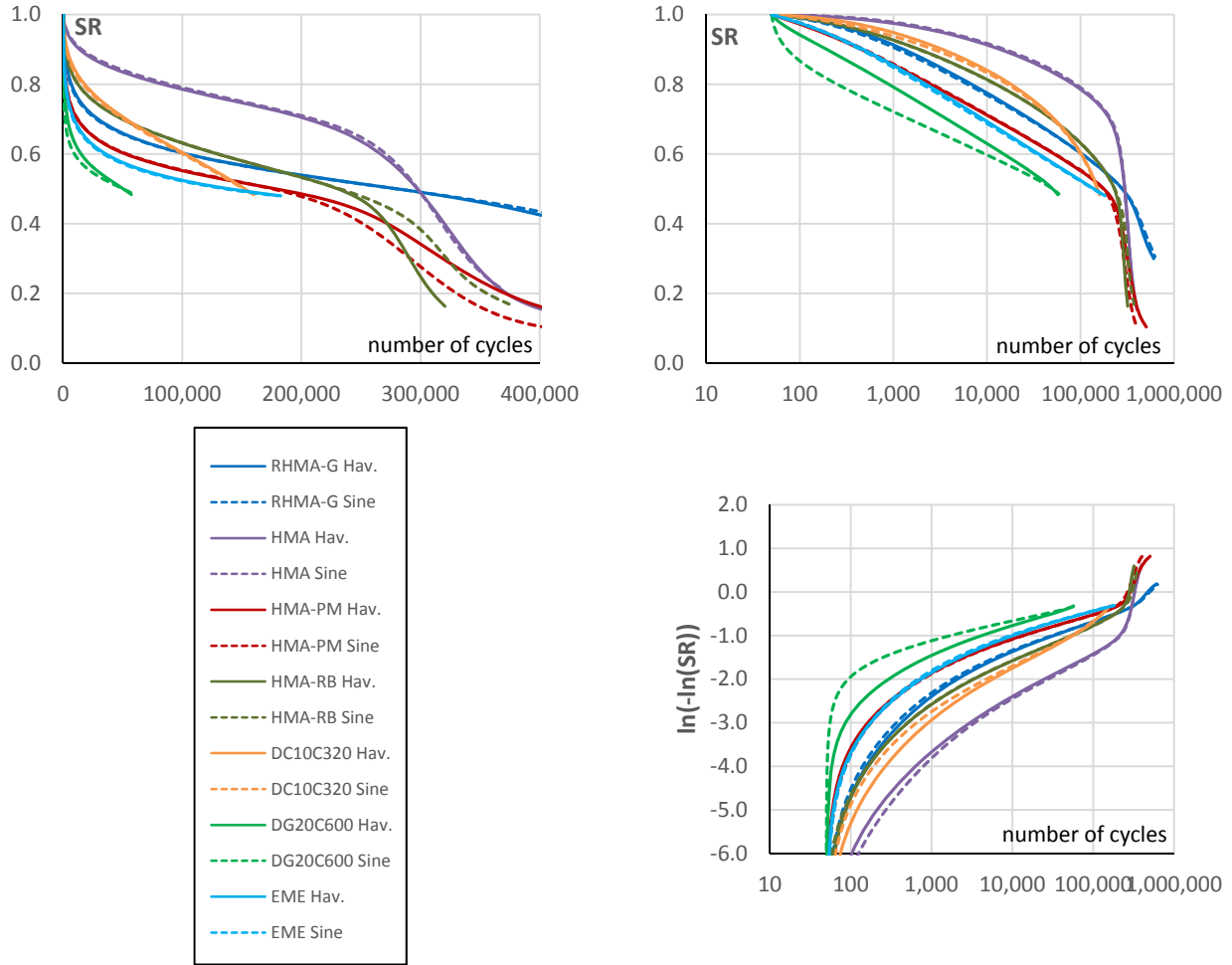
Figure 3.12: Shape of the stiffness degradation curves (SR vs. number of cycles).
(Note: Haversine and sine stiffness degradation curves have been scaled [constant factor cycles axle] so that both coincide at the 50 percent stiffness reduction point.)

3.5 Analysis of Test Results in the Black Space

Damage accumulation in fatigue tests has long been known to be strongly related to dissipated energy *(12)*. Therefore, the joint evolution of dynamic modulus and phase angle, upon which dissipated energy depends, has been plotted in Black space (dynamic modulus versus phase angle evolution during fatigue testing), providing another way to compare the results of haversine versus sine testing. Results from six haversine and sine tests conducted at different strain levels were plotted, with examples shown in Figure 3.13 and Figure 3.14. The figures show that for six of the seven mixtures, the differences between average haversine and sine curves were considerably smaller than the variability between the tests. However, as in the other tests where contradictory results were obtained, for mix DG20 C600 the differences between the average haversine and sine curves were larger than those for the test-to-test variability (see Figure 3.15). For this particular mix, complex modulus evolution follows a different path depending on whether the test is conducted in haversine or sine mode. The main difference comes from the phase angle, which was consistently higher in the sine testing than in the

haversine testing. This higher phase angle appeared in the earliest cycles. This can also be seen in Figure 3.16, where initial dynamic modulus and phase angle are plotted for all mixes. In this figure, each point corresponds to a fatigue test. And again, haversine and sine seem to follow the same pattern for all the mixes except DG20 C600.
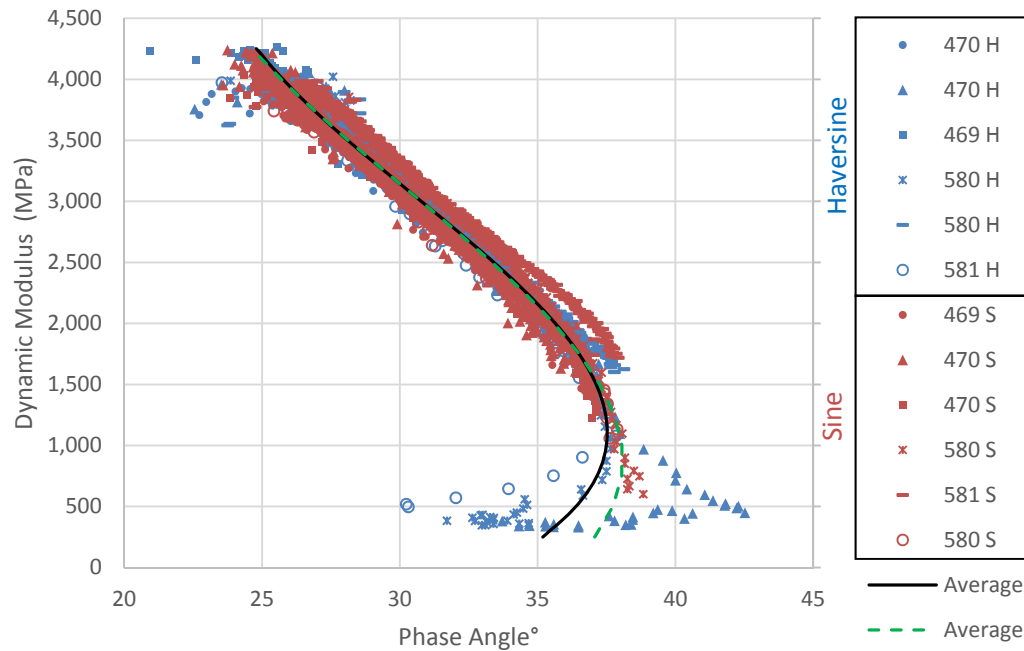
Figure 3.13: Haversine versus sine comparison for mix RHMA-G in a Black space.
(Note: specimen ID includes peak-to-peak strain and S for sine, H for haversine.)
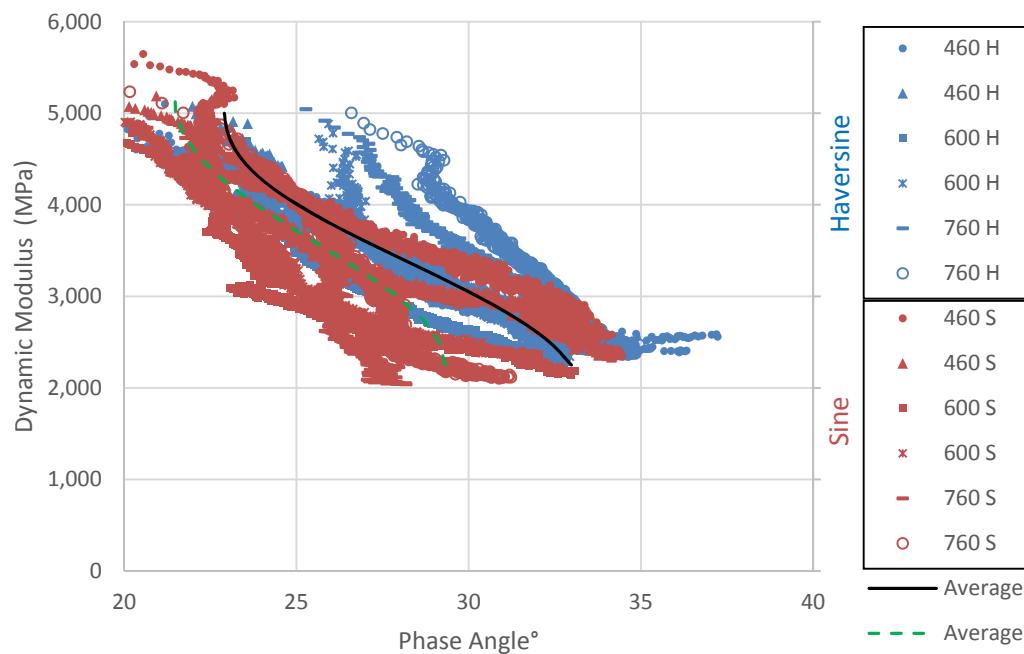
Figure 3.14: Haversine versus sine comparison for mix EME in a Black space.
(Note: specimen ID includes peak-to-peak strain and S for sine, H for haversine.)
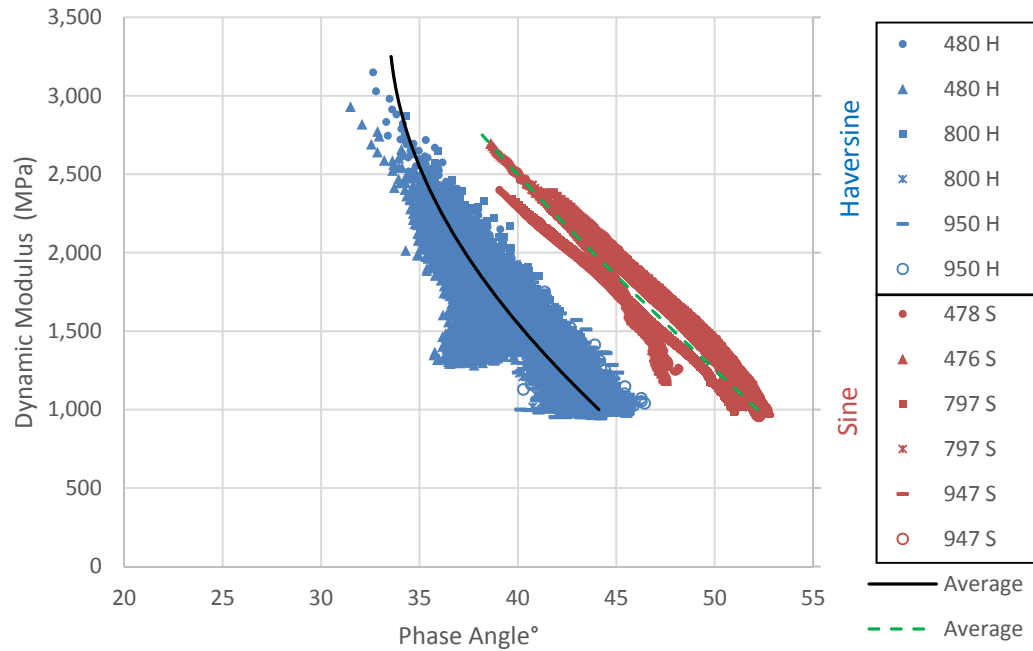
**Figure 3.15: Haversine versus sine comparison for mix DG20 C600 in a Black space.
(Note: specimen ID includes peak-to-peak strain and S for sine, H for haversine.)**
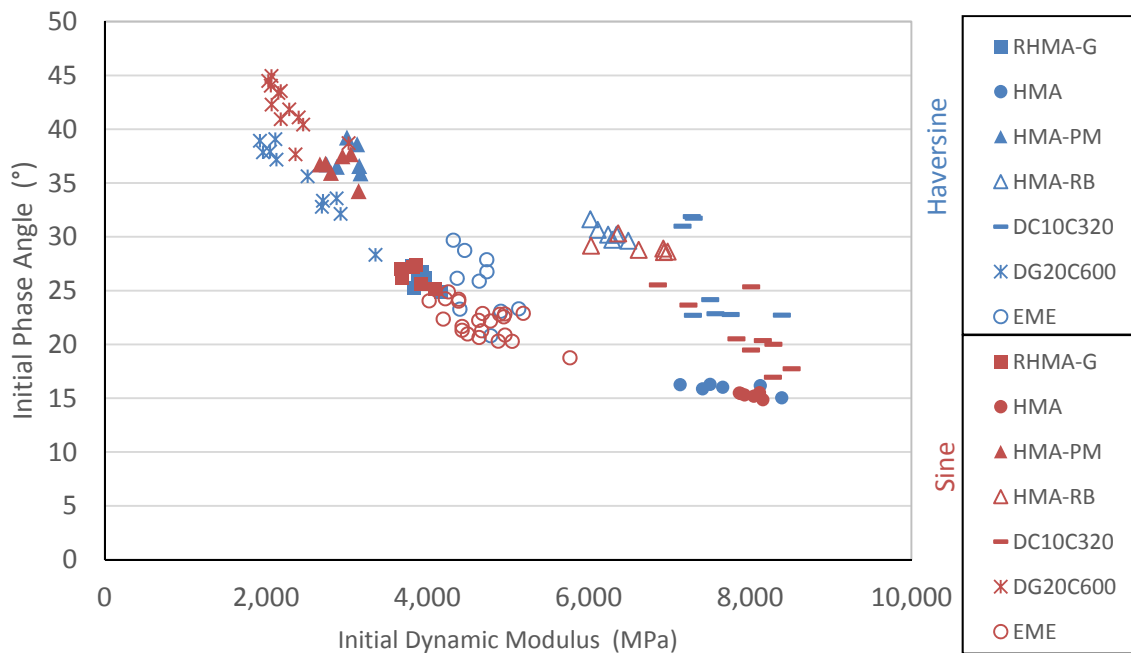
Figure 3.16: Haversine versus sine comparison in terms of initial complex modulus (at 50 load cycles).

3.6 ANOVA Analysis for All Mixes

The ANOVA results presented in Figure 3.10 were obtained for each specific mix independently. In addition to this, an analysis of variance was also conducted for the complete data set in an attempt to capture information that the piecewise comparison missed. The overall analysis includes mix type, test mode (haversine or sine), and strain level, as fixed factors, and log fatigue life as the dependent variable. Mix type and testing mode were regarded as crossed factors, while strain level was regarded as a factor nested in mix type. This is because the meaning of strain level differs from one mix to another.

The ANOVA was first conducted using the 50 percent stiffness reduction fatigue lives, since this was the only failure criterion that could be determined for all the mixes. These ANOVA results are shown in Table 3.2. According to this analysis the test mode effect is not significant, with a p-value=0.105, although the first order interaction "Mix*Test Mode" is significant, with a p-value=0.003. This indicates that the test mode effect may vary among the different mixtures, which is in line with the significance levels obtained for the individual mixes. As shown above (Figure 3.10), test mode was significant only for mix DG20 C600. The Mix*Test Mode interaction can also be seen in Figure 3.19, which is a plot created by *SPSS* software that was used for this statistical analysis.

A second analysis that did not include mix DG20 C600 was also conducted, and its results are presented in Table 3.3. In this second ANOVA, neither test mode (p-value=0.955) nor its interaction with mix type (p-value=0.438) is significant. This indicates that haversine and sine did not result in statistically different 50 percent stiffness reduction fatigue lives.

The fact that the ANOVA was conducted using the 50 percent stiffness reduction fatigue lives was considered a limitation, since this failure criteria was regarded as somewhat arbitrary and not tied to a change of the damage phenomenon. The reason why this failure criterion was regarded as arbitrary is the transition from phase II to phase III of fatigue testing that can be regarded as the "true failure," meaning the transition from dispersed microcracking damage to the formation of distinct cracks does not necessarily take place when the stiffness of the specimen reduces by 50 percent. The 50 percent stiffness reduction criterion was originally selected in the 1960s as a convenient and easy to calculate parameter based on observations of the deformation-controlled testing of conventional hot mix asphalt at the time.

The transition point between phases II and III was determined for the tests where both phases II and III took place (mixes tested at the UCPRC beyond 50 percent stiffness reduction). An objective criterion does not currently exist that delimits the transition between both phases. For this research, the transition point was

determined as the point where the curvature radius of the curve "stiffness versus number of cycles" reaches a minimum (see example determination in Figure 3.17). The stiffness ratio at this transition point was compared to the stiffness ratio obtained using each of the three alternative failure criteria (50 and 60 percent stiffness reduction and maximum of |E*|xn). Results of this comparison are presented in Figure 3.18. This figure shows that the stiffness ratio at this transition point is mix dependent, being higher in standard HMA mixes with plain asphalt binders than in mixes with rubber or polymer-modified binders or in Rich Bottom HMA mixes with high binder content and an air-void content less than three percent.

Figure 3.18 shows that the $|E*| \times n$ failure criterion was much closer to true failure than the other two failure criteria were. For this reason, a third ANOVA was conducted using fatigue lives determined according to $|E*| \times n$ failure criteria. Only mixes tested at the UCPRC could be included in this third ANOVA, since Australian mixes were tested up to 50 percent stiffness reduction and, in most cases, the maximum of the curve stiffness multiplied by the number of cycles ($|E*| \times n$) did not take place. Results of this third analysis, shown in Table 3.4, indicate the test mode effect is not significant, with a p-value=0.988. Test mode significance levels did not change much (p-value=0.965) when extrapolated data from mix DG C320 was included in the analysis. As explained above, DG C320 was the only Australian mix where $|E*| \times n$ failure points could be determined using extrapolation.

The mean square error of the ANOVA analysis was 0.04 (0.20 standard deviation) when the failure criterion was 50 percent stiffness reduction, and it was 0.068 (0.26 standard deviation) when max of $|E*| \times n$ failure criterion was used. These values are somewhat smaller than the repeatability standard deviation of 0.278 reported by ASTM D7460-10.
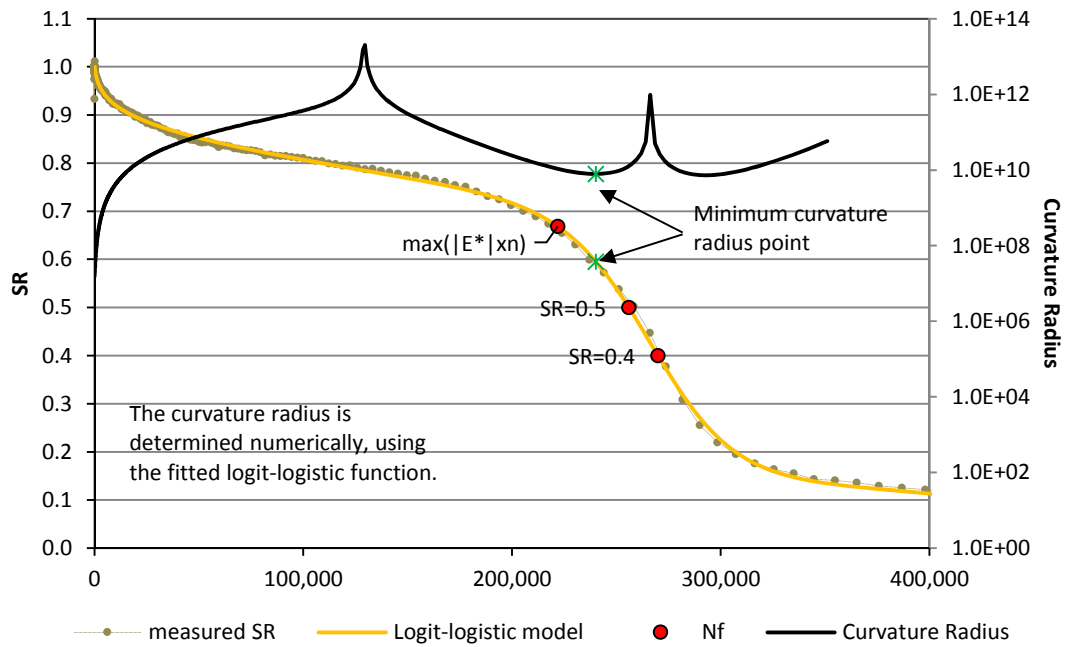
Figure 3.17: Example of transition point between phases II and III (HMA, specimen 6S, 316 µε peak to peak).
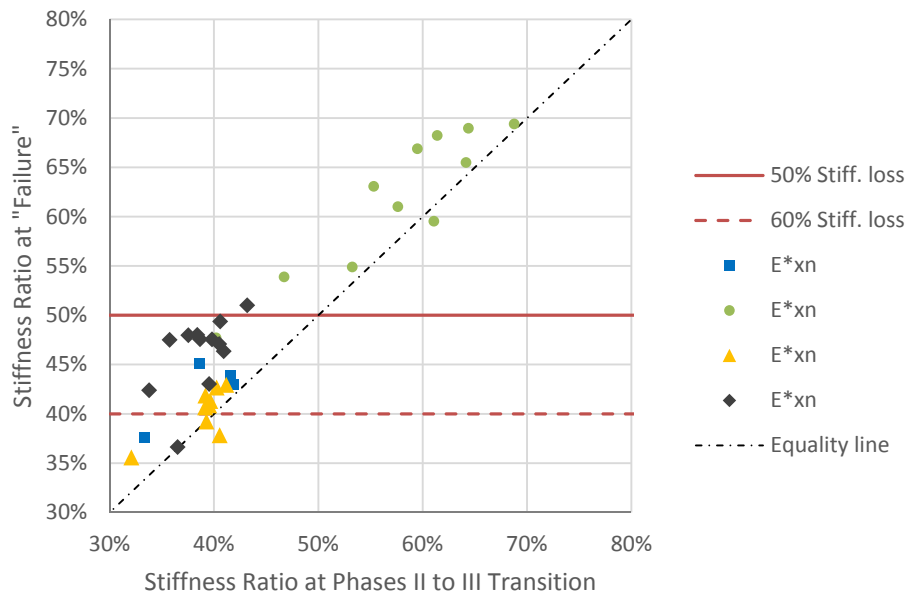
Figure 3.18: Stiffness ratio at failure, according to the three failure criteria (50 and 60 percent stiffness reduction and maximum of |E*|×n).

Table 3.2: ANOVA Results, All Mixes, 50% Stiffness Loss Failure Criterion

Tests of Between-Subjects Effects					
Dependent Variable: log(Nf-50%)					
Source	Type III Sum of Squares	df	Mean Square	F	Sig.
Corrected Model	53.435[a]	33	1.619	40.358	.000
Intercept	2969.084	1	2969.084	74001.341	.000
Mix	7.022	6	1.170	29.168	.000
Mode	.108	1	.108	2.689	.105
Strain(Mix)	42.110	10	4.211	104.956	.000
Mix * Test Mode	.899	6	.150	3.733	.003
Test Mode * Strain(Mix)	.162	10	.016	.403	.941
Error	3.210	80	.040		
Total	3281.629	114			
Corrected Total	56.645	113			
a. R Squared =.943 (Adjusted R Squared =.920)					
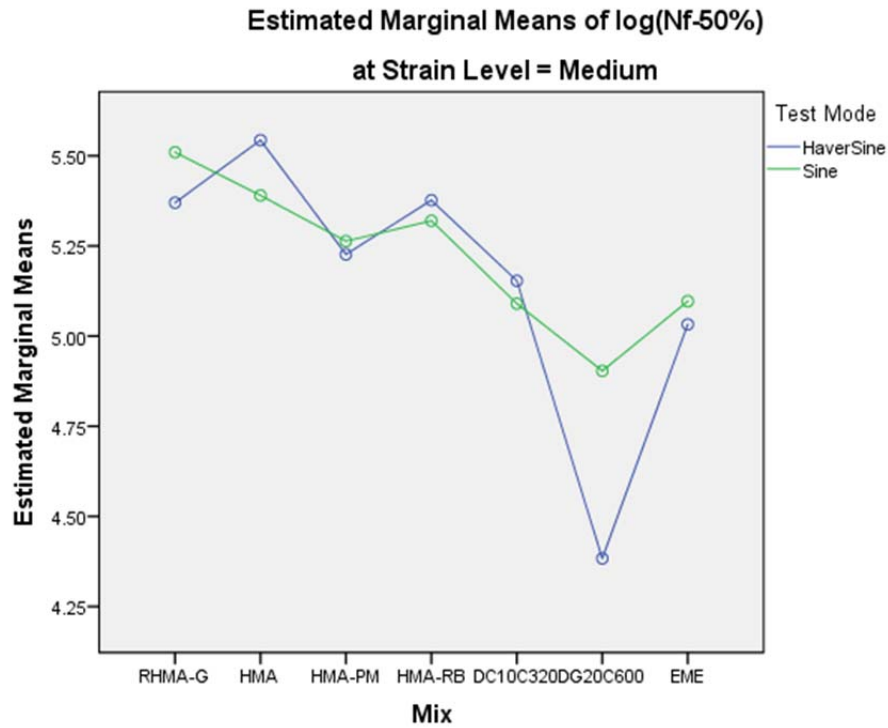
Figure 3.19: Haversine versus sine comparison, all mixes, medium strain level: dependent variable is number of cycles to 50% stiffness reduction.

Table 3.3: ANOVA Results, not Including Mix DG20 C600, 50% Stiffness Loss Failure Criterion

Tests of Between-Subjects Effects					
Dependent Variable: log(Nf-50%)					
Source	Type III Sum of Squares	df	Mean Square	F	Sig.
Corrected Model	40.903[a]	27	1.515	36.300	.000
Intercept	2510.153	1	2510.153	60146.096	.000
Mix	4.390	5	.878	21.037	.000
Mode	.000	1	.000	.003	.955
Strain(Mix)	32.436	8	4.054	97.149	.000
Mix * Mode	.204	5	.041	.980	.437
Mode * Strain(Mix)	.146	8	.018	.438	.894
Error	2.796	67	.042		
Total	2794.171	95			
Corrected Total	43.700	94			
a. R Squared =.936 (Adjusted R Squared =.910)					

Table 3.4: ANOVA Results, Californian Mixes, |E*|xn Failure Criterion

Tests of Between-Subjects Effects					
Dependent Variable: log(Nf-E*xn)					
Source	Type III Sum of Squares	df	Mean Square	F	Sig.
Corrected Model	3.622a	16	.226	2.622	.015
Intercept	1112.663	1	1112.663	12887.890	.000
Mix	2.009	4	.502	5.819	.002
Mode	1.856E-05	1	1.856E-05	.000	.988
Strain(Mix)	1.376	4	.344	3.984	.012
Mix * Mode	.227	3	.076	.876	.467
Mode * Strain(Mix)	.022	4	.005	.064	.992
Error	2.158	25	.086		
Total	1342.122	42			
Corrected Total	5.780	41			
a. R Squared =.627 (Adjusted R Squared =.388)					

4 DISCUSSION OF RESULTS

The analyses presented above showed no differences between the haversine and sinusoidal testing mode results for six of the seven asphalt mixtures evaluated in this study. For these six mixes, the haversine and sinusoidal fatigue lives did not seem to differ from each other when plotted versus strain in a double logarithmic graph (classical plot log Nf versus log strain). In particular, the 90 percent confidence intervals determined for ε_6 for the haversine and sinusoidal testing modes overlapped. The slope of the fatigue law (log Nf – log ε linear relationship) and the fitting error were similar between the haversine and sinusoidal testing modes even though both parameters changed considerably from one mix to another. The ANOVA analyses did not show statistically significant differences between the two testing modes, in terms of the fatigue lives determined for three different failure criteria, for these six mixes. In addition, the shapes of the stiffness degradation curves (SR versus number of cycles) were almost identical when the haversine and sinusoidal testing modes were compared to each other. A similar conclusion was reached when the joint evolution of dynamic modulus and phase angle during fatigue testing (Black diagrams) was considered for these six mixes.

This similar performance is believed to be strongly related to the viscoelastic nature of the asphalt mix. Because of mix viscoelastic behavior, a flexural bending test that is initiated under a haversine waveform rapidly changes into a sinusoidal waveform conducted on a bent beam. This rapid change is shown in an example in Figure 4.1. The initial peak downward load is higher in the haversine case, since initial displacement (versus zero position) is twice the value of the sine test. Nonetheless, the asphalt mix flows due to its viscoelastic nature so the beam at-rest position will progressively deflect too. Consequently, the load required to bend the beam to the maximum deflection will lessen while a negative force will be required to bring the beam back to the original at-rest position.

A similar load evolution has been described before *(6)*. After a number of cycles, around 50 in the example shown in Figure 4.1, the beam at-rest position will be half way between zero and maximum deflection, so the force required to reach both extremes will be the same magnitude but with the opposite sign. This means that, stress-wise, there is no difference between haversine and sine fatigue testing after a number of cycles have been applied. Two different specimens are compared in Figure 4.1, which explains peak-to-peak load differences. The fact that initial stiffness and phase angle (determined at cycle 50) are similar between haversine and sine testing (Figure 3.16) supports the observation that transition from haversine to "sine on deflected beam" takes place very rapidly, i.e., the beam rapidly "forgets" what its original position was.

As has been shown in all the results, one of the seven mixtures tested, DG20 C600, yielded a different set of conclusions in the sine-versus-haversine comparison. DG20 C600 is a dense-graded Australian mix typically

used as a base layer, and it was tested at 30°C. For this particular mix, sinusoidal testing resulted in considerably longer fatigue lives than haversine testing (one to two times longer). These differences were shown to be statistically significant. The shape of the stiffness degradation curves showed clear differences between the haversine and sine testing modes for this particular mix. Clear differences were also observed in the Black space, since phase angle was systematically higher in sinusoidal testing compared to the haversine.

No definitive explanation was found for the performance of this mix. In particular, the transition from haversine to "sine on deflected beam" was verified for this mix, as reflected in the example shown in Figure 4.2. Note that upward and downward loading are almost identical after ten cycles.

It is important to bear in mind that the key to the similarity between haversine and sine testing is the viscoelastic nature of the asphalt mix. Beam flexural testing conducted at low temperatures or on mixes whose binder has undergone considerable aging may be sensitive to whether haversine or sinusoidal displacement mode is used. Something similar might happen for very hard binders tested at intermediate and low temperatures. However, none of these possible explanations apply to mix DG20 C600.
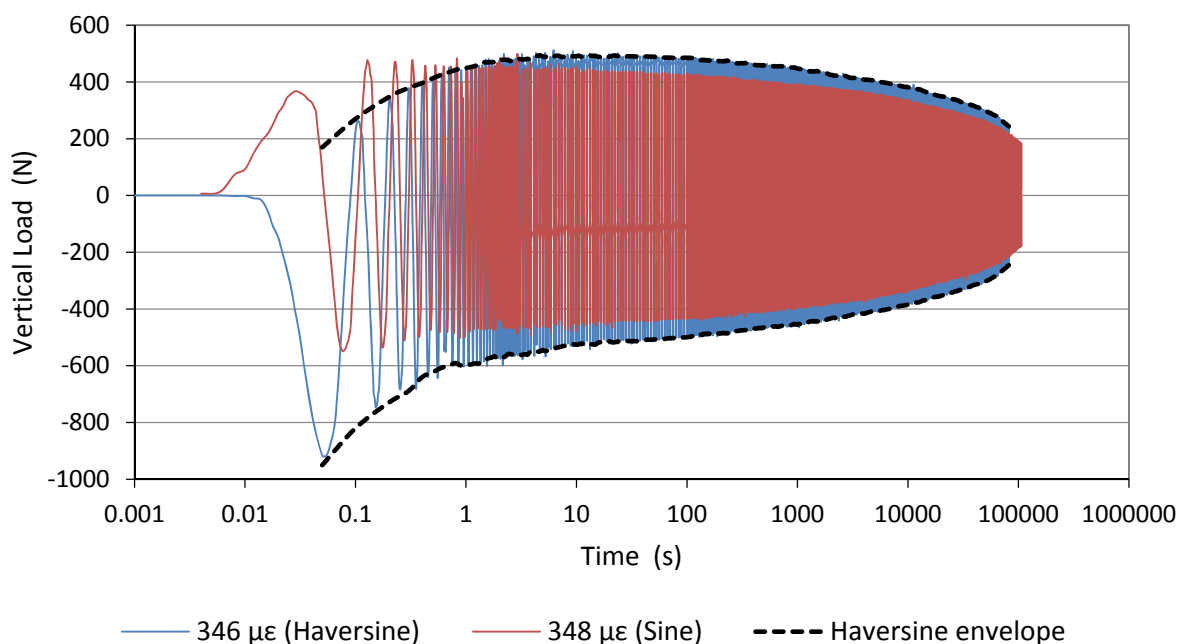
Figure 4.1: Evolution from haversine to "sine on deflected beam" (HMA-RB, 350 με peak to peak).
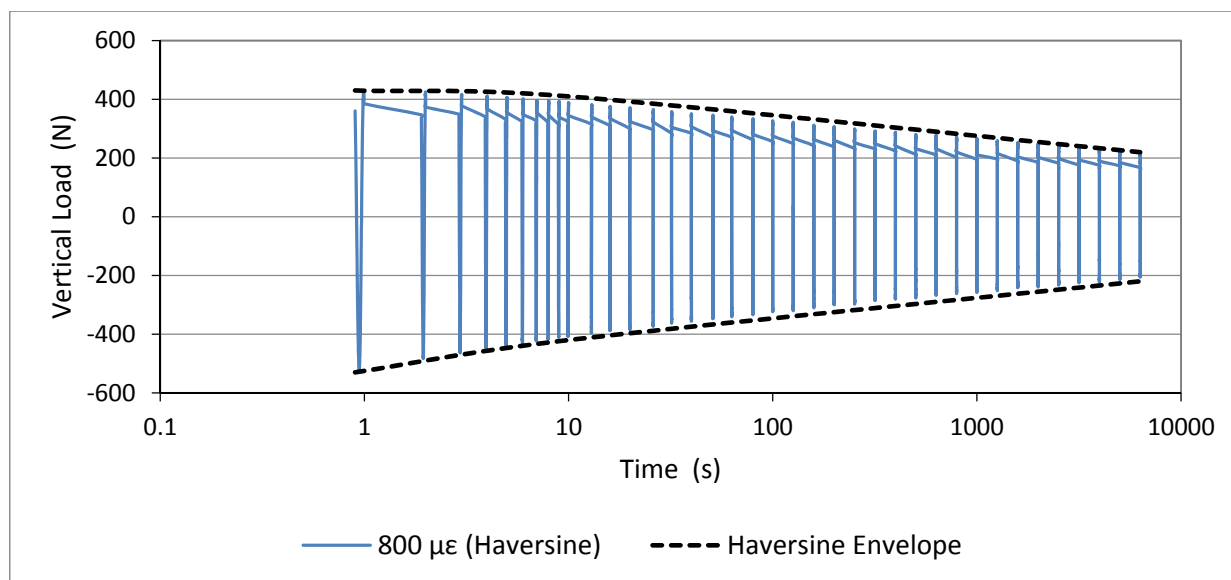
Figure 4.2: Evolution from haversine to "sine on deflected beam" (DG20 C600, 800 με peak to peak).
(Note: load was not recorded for all cycles.)

The haversine waveform has traditionally been considered to reproduce field conditions better than the sinusoidal waveform because the passing of a truck mainly pushes a pavement in the downward direction. Lately, some concerns have been raised about testing in haversine mode, since "test assumptions do not match the actual test conditions" *(4)*. Actually, the same beam theory has been used to determine asphalt strain in the ASTM D7460-10 and AASHTO T 321-14 standards. According to this theory, and assuming third-point loading, null specimen weight, and constant asphalt stiffness along the beam as well, strain is automatically determined after beam dimensions and center deflection are set. The same is applicable to the stress, which is determined from the load level and beam dimensions. Possible confusion could be avoided if ASTM specifically indicated that the load referred to is the peak-to-peak value, as is indicated in AASHTO T 321-14.

Concerns have also been raised about the applicability of haversine testing when rest periods are introduced between pulse loads *(4)*. This concern is based on the shape of the stress pulses, which are not sinusoidal when rest periods are introduced in haversine testing. Again, this is related to the viscoelastic nature of the asphalt mix. Since asphalt relaxes during rest periods, the "bent beam" state halfway between zero and maximum deflection is never reached. Because of this, every haversine pulse causes a stress that is almost as high as in the first pulse (Figure 4.1). For this reason, a balance exists between the stiffness recovery, attributable to thixotropy or healing, that takes place during rest periods and the higher damage due to the higher stress pulses.

Reference *(4)* shows that the result of this balance is not obvious, and that shorter fatigue lives may be obtained when rest periods are introduced in haversine testing. This runs against traditional observations of the effect of

rest periods *(13).* It is important to bear in mind that this balance also takes place on real roads, where bending of the neutral axis of the asphalt pavement and stiffness recovery have opposite dependencies on the rest periods between axle loads. The first one decreases and the second one increases with increasing rest periods. Consequently, haversine testing with rest periods, although more difficult to understand and analyze than its sinusoidal counterpart, may be more realistic.

Regarding the definition of failure in the 4PFBF test, it was found for those mixes that could be compared that the maximum $|E^*| \times n$ criterion is more related to the physical phenomenon of microcracking beginning to propagate through the beam compared with the criterion of 50 percent loss of initial stiffness that has been used in Caltrans performance-related specifications to date. The $|E^*| \times n$ criterion is therefore also better able to represent the "failure" of the mix in fatigue and should be a more consistent parameter for fatigue failure particularly when comparing conventional, polymer-modified and rubberized mixes.

5 SUMMARY, CONCLUSIONS, AND RECOMMENDATIONS

5.1 Summary

An experimental study was conducted to determine the effect of deflection waveform on fatigue test results for hot mix asphalt. Seven asphalt mixtures, comprising a wide variety of gradations, binder types, and binder contents were selected for this study. Four of the mixes were tested at the UCPRC, and three were tested by the Australian ARRB Group. The mixes were tested at different strain levels under both haversine and sinusoidal deflection-controlled modes, without introducing rest periods between load cycles. Results from the two testing modes were compared from different perspectives. This comparison allowed a detailed evaluation of the effects each testing mode has on fatigue testing results. The following was observed:

- For six of the seven mixes, no evidence was found to indicate that the haversine and sinusoidal testing modes resulted in different beam stiffness degradation. Fatigue life, the shape of the stiffness reduction curves, initial dynamic moduli and phase angles, and Black diagrams were essentially the same under both displacement modes. The reason for the similarity of the results from haversine and sinusoidal testing is attributable to the viscoelastic nature of the asphalt mix. Experimental data showed that haversine tests rapidly change into sinusoidal tests conducted on a bent beam, so the same stress is produced by haversine and sinusoidal deflection waveforms as soon as the peak-to-peak deflection amplitudes are equal. These findings indicate that haversine displacement control testing using the ASTM protocol in effect results in a sinusoidal stress response of half the intended amplitude.

- For one of the seven mixes, sinusoidal testing produced considerably longer fatigue lives than haversine testing (one to two times longer). No definitive explanation was found for the outcome of the testing on this mix, whose performance differed considerably from the performance of the other six mixes.

5.2 Conclusions

Based on these results, it was concluded that there is no compelling reason to recommend that the UCPRC change from a haversine to a sinusoidal mode of testing. On the other hand, if the ASTM and AASHTO tests are harmonized to require a sinusoidal mode of loading, no reason was found not to make this change. This is because the same fatigue life and stiffness degradation curves are expected from the two testing modes when rest periods are not included between loading cycles.

These results imply that if the UCPRC were to change to sinusoidal testing from haversine testing, none of the historical fatigue model parameters calibrated by UCPRC would need to be adjusted. One reason to move to the sinusoidal mode of testing is that, in terms of stress, haversine testing becomes sinusoidal after some number of cycles has been applied. This change in the shape of the stress pulse does not occur with sinusoidal testing since the stress pulse is sinusoidal from the beginning of the fatigue test.

It must be noted that the results obtained in this experimental study should not be extrapolated to conditions where the viscoelastic nature of the asphalt mix has been severely limited; examples of these conditions include testing the mix at low temperatures or conducting tests on mixes with very hard binders or whose binder has undergone considerable aging. Under these conditions, 4PFBF test results may indeed be sensitive to whether haversine or sinusoidal displacement is used.

5.3 Recommendations

It is recommended that the UCPRC change to sinusoidal loading if there are indications that the ASTM and AASHTO test methods will be harmonized to use that mode of loading. It is recommended that if this change occurs that no adjustments be made to past data or *CalME* models. If testing is to include specimens or conditions under which the material is much more elastic and less viscoelastic, as might occur at colder temperatures or with very aged mixes, the conclusions and recommendations from this study should be checked with further testing and analysis. It is also recommended that consideration be given to defining failure in Caltrans performance-related specifications using the $|E^*| \times n$ criterion instead of the currently used criterion of 50 percent loss of initial stiffness.

REFERENCES

1. Tayebali, A. et al. 1994. *Fatigue Response of Asphalt-Aggregate Mixes*, Report No.: SHRP-A-404. Prepared by Asphalt Research Program, Institute of Transportation Studies, University of California, Berkeley for the Strategic Highway Research Program.

2. ASTM D7460-10. 2010. *Standard Test Method for Determining Fatigue Failure of Compacted Asphalt Concrete Subjected to Repeated Flexural Bending*.

3. AASHTO T 321-14. 2014. *Standard Method of Test for Determining the Fatigue Life of Compacted Asphalt Mixtures Subjected to Repeated Flexural Bending*.

4. Mamlouk, M.S., M.I. Souliman, W.A. Zeiada, and K.E. Kaloush. 2012. *Refining Conditions of Fatigue Testing of Hot Mix Asphalt.* Advances in Civil Engineering Materials. Vol. 1, No. 1: pp. 1-13.

5. EN 12607-24:2012. 2012. *Bituminous Mixtures – Test Methods for Hot Mix Asphalt – Part 24: Resistance to Fatigue*.

6. Pronk, A.C., M.R. Poot, M.M.J. Jacobs, and R.F. Gelpke. 2010. *Haversine Fatigue Testing in Controlled Deflection Mode: Is It Possible?*, in Transportation Research Board 89th Annual Meeting, No. 10-0485.

7. Mateos, A., J. Ayuso, and B. Jáuregui. 2011. *Shift Factors for Asphalt Fatigue from Full-Scale Testing.* Transportation Research Record: Journal of the Transportation Research Board 2225: pp. 128-136.

8. Criqui, W.B., and C.D. Wendell. 2012. *Flexural Beam Fatigue Equipment Nomenclature Issues*, in The Third Conference on Four-Point Bending. Davis, California.

9. Rowe G.M., and M.G. Bouldin. 2000. *Improved Techniques to Evaluate the Fatigue Resistance of Asphaltic Mixtures.* Proceedings of 2nd Eurasphalt and Eurobitume Congress, Vol. 1, pp. 754-763. Barcelona.

10. Di Benedetto, H., C. De La Roche, H. Baaj, A. Pronk, and R. Lundström. 2004. *Fatigue of Bituminous Mixtures.* Materials and Structures, Vol. 37, No. 3:pp. 202-216.

11. Mateos, A., Wu, R., Harvey, J., Denneman, E. and Fan, A., 2017. The Logit Model and the Need to Reproduce the Stiffness Degradation Curve of Asphalt Specimens During Fatigue Testing. Transportation Research Record: Journal of the Transportation Research Board, (2631), pp.105-113.

12. Van Dijk, W., and W.Visser. 1977. Energy Approach to Fatigue for Pavement Design. Association of Asphalt Paving Technologists Proceedings, Vol. 46, pp. 1-40.

13. Bonnaure, F.P., A.H.J.J. Huibers, and A. Boonders. 1982. A Laboratory Investigation of the Influence of Rest Periods on the Fatigue Response of Bituminous Mixes. Association of Asphalt Paving Technologists Proceedings, Vol. 51, p. 104-128.

APPENDIX A: SUMMARY OF TEST RESULTS

Mix ID	Specimen ID	Initial Modulus (MPa)	Initial Phase Angle (°)	Peak-to-Peak Strain (με)	Failure Point			Test Mode	Strain Level
					Nf SR=50%	Nf SR=40%	Nf Max (|E*|xn)		
RHMA-G	1H	3,833	25.3	469.7	2,985,381			Haversine	Low
RHMA-G	8H	3,976	26.2	470.2	728,617	1,090,183	999,999	Haversine	Low
RHMA-G	7H	4,168	24.9	469.0	728,617			Haversine	Low
RHMA-G	41H	3,939	26.7	579.8	177,826	237,136	217,519	Haversine	Medium
RHMA-G	2H	3,816	27.3	580.1	362,192	789,640		Haversine	Medium
RHMA-G	11H	3,887	26.4	581.0	199,525	398,106	421,695	Haversine	Medium
RHMA-G	6S	3,684	26.2	469.4	1,539,925	3,072,556		Sine	Low
RHMA-G	8S	4,090	25.1	470.2	486,966	865,963		Sine	Low
RHMA-G	2S	3,921	25.6	470.0	1,122,017	1,995,261	2,304,091	Sine	Low
RHMA-G	5S	3,822	27.2	579.5	251,187	354,812	325,460	Sine	Medium
RHMA-G	4S	3,856	27.4	581.1	461,421	1,268,243		Sine	Medium
RHMA-G	7S	3,670	27.0	579.8	298,537	595,661	630,956	Sine	Medium
HMA	4H	8,395	15.0	266.1	1,295,685	1,539,925	1,258,924	Haversine	Low
HMA	8H	7,412	15.9	267.5	749,193	777,448	653,169	Haversine	Low
HMA	2H	7,663	16.0	268.2	459,725	478,488	409,731	Haversine	Low
HMA	22H	7,506	16.3	315.5	414,744	451,537	391,578	Haversine	Medium
HMA	34H	8,130	16.2	315.6	434,009	515,821	459,725	Haversine	Medium
HMA	1H	7,135	16.3	315.7	236,318	252,019	198,634	Haversine	Medium
HMA	3S	8,160	14.9	265.4	546,385	578,760	486,966	Sine	Low
HMA	33S	8,119	15.5	266.6	535,436	590,735	456,226	Sine	Low
HMA	5S	7,869	15.5	267.2	334,964	421,695	244,060	Sine	Low
HMA	7S	8,048	15.2	315.4	365,173	409,731	334,964	Sine	Medium
HMA	23S	7,884	15.4	315.5	158,553	167,878	139,971	Sine	Medium
HMA	6S	7,933	15.3	316.0	256,020	269,960	221,888	Sine	Medium
HMA-PM	10H	3,173	35.9	505.9	302,847	457,521	481,193	Haversine	Low
HMA-PM	13H	2,752	36.7	513.2	154,242	246,898	262,527	Haversine	Low
HMA-PM	17H	3,130	38.6	504.0	666,163	1,681,652	2,045,571	Haversine	Low
HMA-PM	1H	3,157	36.6	706.9	97,161	149,622	145,377	Haversine	
HMA-PM	3H	3,003	39.2	658.9	97,161	158,488	153,991	Haversine	Medium
HMA-PM	7c1S	2,668	36.7	504.6	81,751	129,567	129,567	Sine	Low
HMA-PM	7c2S	2,738	36.8	503.5	503,646	1,135,665		Sine	Low
HMA-PM	11S	3,148	34.3	502.9	865,963	1,883,648	2,113,488	Sine	Low
HMA-PM	8S	3,052	37.7	655.3	281,837	459,725	434,009	Sine	Medium
HMA-PM	12S	2,806	35.9	655.5	244,060	316,226	298,537	Sine	Medium
HMA-PM	15S	2,949	37.5	655.5	89,124	133,351	129,567	Sine	Medium
HMA-RB	8H	6,345	30.2	346.3	459,725	546,385	473,150	Haversine	Low
HMA-RB	19H	6,491	29.6	348.1	578,760	630,956	578,760	Haversine	Low
HMA-RB	21H	6,293	29.7	345.6	546,385	630,956	562,340	Haversine	Low
HMA-RB	12H	6,240	30.2	428.8	217,519	251,187	223,871	Haversine	Medium
HMA-RB	20H	6,113	30.7	428.2	295,883	345,026	317,273	Haversine	Medium
HMA-RB	22H	6,020	31.6	423.9	211,347	258,522	230,408	Haversine	Medium
HMA-RB	9S	6,029	29.2	348.4	709,007	1,058,311	1,169,166	Sine	Low
HMA-RB	11S	6,926	28.9	345.0	668,342	841,394	794,327	Sine	Low
HMA-RB	17S	6,979	28.6	346.7	397,591	438,374	390,471	Sine	Low
HMA-RB	10S	6,366	30.3	427.5	244,060	334,964	316,226	Sine	Medium
HMA-RB	13S	6,933	28.6	425.9	188,363	230,408	199,525	Sine	Medium
HMA-RB	14S	6,620	28.8	428.0	199,891	243,740	220,964	Sine	Medium
DC10C320	S13B3H	8,394	22.7	199.9	3,054,123	3,307,352	2,934,856	Haversine	Low
DC10C320	S4B3H	7,759	22.8	202.8	4,113,345	4,965,952	4,243,163	Haversine	Low
DC10C320	7B1H	7,293	22.7	399.9	161,047	198,597	178,110	Haversine	Medium
DC10C320	14B3H	7,505	24.2	399.9	120,117	151,036	137,476	Haversine	Medium
DC10C320	S2B4H	7,572	22.9	399.9	148,064	192,757	180,793	Haversine	Medium
DC10C320	S2B2H	7,279	31.9	800.2	6,270			Haversine	High

Mix ID	Specimen ID	Initial Modulus (MPa)	Initial Phase Angle (°)	Peak-to-Peak Strain (µε)	Failure Point			Test Mode	Strain Level
					Nf SR=50%	Nf SR=40%	Nf Max (|E*|xn)		
DC10C320	S3B3H	7,162	31.0	800.1	6,902	9,519	9,757	Haversine	High
DC10C320	S20B3H	7,302	31.7	800.1	8,181	12,253	13,850	Haversine	High
DC10C320	S5B2S	8,516	17.8	200.0	2,963,013	3,529,519	3,150,727	Sine	Low
DC10C320	S7B4S	8,159	20.4	200.1	4,568,727			Sine	Low
DC10C320	S12B2S	8,284	17.0	200.0	4,060,088	5,097,363	4,634,990	Sine	Low
DC10C320	S17B1S	8,290	20.0	399.8	134,898	176,440	166,943	Sine	Medium
DC10C320	S2B3S	7,832	20.5	400.1	106,444	131,605	118,211	Sine	Medium
DC10C320	S3B2S	8,013	19.5	400.1	130,134	169,093	158,907	Sine	Medium
DC10C320	15B1S	6,857	25.5	800.4	8,699	12,379	13,738	Sine	High
DC10C320	27B3S	8,015	25.4	800.2	5,057	6,780	6,763	Sine	High
DC10C320	S20B4S	7,237	23.7	800.3	7,331	10,328	10,600	Sine	High
DC20C600	190-3H	3,357	28.3	240.0	5,309,576			Haversine	
DC20C600	213-2H	2,875	33.6	480.0	338,985			Haversine	Low
DC20C600	213-3H	2,692	32.8	480.0	1,038,934			Haversine	Low
DC20C600	213-4H	2,706	33.4	480.0	809,664			Haversine	Low
DC20C600	213-5H	2,925	32.1	480.0	331,321			Haversine	Low
DC20C600	212-2H	2,515	35.6	800.0	14,275			Haversine	Medium
DC20C600	212-4H	2,128	37.2	800.0	48,490			Haversine	Medium
DC20C600	212-5H	1,962	37.9	800.0	20,230			Haversine	Medium
DC20C600	190-4H	1,924	38.9	950.0	18,716			Haversine	High
DC20C600	190-5H	2,050	37.9	950.0	10,678			Haversine	High
DC20C600	212-1H	2,115	39.1	950.0	11,354			Haversine	High
DC20C600	187-4S	2,366	37.7	397.8	2,293,018			Sine	
DC20C600	189-5S	3,023	38.7	476.8	1,595,658			Sine	Low
DC20C600	190-1S	2,461	40.4	476.4	1,195,164			Sine	Low
DC20C600	190-2S	2,183	40.9	477.5	1,399,619			Sine	Low
DC20C600	187-5S	2,288	41.9	598.1	407,519			Sine	
DC20C600	188-1S	2,405	41.1	697.5	124,657			Sine	
DC20C600	188-2S	2,070	42.3	797.1	100,674			Sine	Medium
DC20C600	189-2S	2,152	43.4	797.0	67,350			Sine	Medium
DC20C600	189-4S	2,182	43.6	796.8	76,467			Sine	Medium
DC20C600	189-1S	2,067	45.0	946.6	30,952			Sine	High
DC20C600	188-5S	2,059	44.1	947.3	36,526			Sine	High
DC20C600	188-4S	2,028	44.5	947.7	30,940			Sine	High
EME	3427-1H	5,133	23.3	460.0	424,940			Haversine	Low
EME	3427-2H	4,911	23.1	459.9	926,110			Haversine	Low
EME	3427-3H	4,786	20.8	460.0	977,230			Haversine	Low
EME	3427-4H	4,404	23.3	600.0	187,640			Haversine	Medium
EME	3656-1H	4,644	25.9	600.0	61,650			Haversine	Medium
EME	3656-2H	4,370	26.2	600.0	132,840			Haversine	Medium
EME	3656-4H	4,464	28.7	600.0	89,810			Haversine	Medium
EME	3314-3H	4,738	26.8	760.1	26,770			Haversine	High
EME	3314-4H	4,736	27.9	760.0	29,890			Haversine	High
EME	3656-3H	4,323	29.7	760.1	20,780			Haversine	High
EME	3329-1S	5,769	18.8	430.2	964,816			Sine	
EME	3342-3S	4,638	22.2	430.2	3,525,513			Sine	
EME	3355-2S	5,052	20.3	460.3	989,819			Sine	Low
EME	3356-3S	5,189	22.9	460.3	681,293			Sine	Low
EME	3359-3S	4,783	22.2	460.3	1,107,757			Sine	Low
EME	3359-4S	4,962	20.9	460.2	2,356,255			Sine	Low
EME	3361-2S	4,023	24.0	460.3	2,464,148			Sine	Low
EME	3405-4S	4,262	24.9	460.3	1,689,577			Sine	Low
EME	3399-1S	4,686	22.9	460.3	2,729,677			Sine	Low
EME	3400-1S	4,387	24.0	460.3	857,696			Sine	Low
EME	3315-2S	4,643	20.7	600.3	152,914			Sine	Medium

Mix ID	Specimen ID	Initial Modulus (MPa)	Initial Phase Angle (°)	Peak-to-Peak Strain (με)	Failure Point Nf SR=50%	Failure Point Nf SR=40%	Failure Point Nf Max (|E*|xn)	Test Mode	Strain Level
EME	3339-2S	4,500	21.0	600.4	112,490			Sine	Medium
EME	3339-3S	4,432	21.7	600.3	132,502			Sine	Medium
EME	3339-4S	4,432	21.3	600.4	157,681			Sine	Medium
EME	3342-1S	4,880	20.3	600.3	87,768			Sine	Medium
EME	3342-2S	4,673	21.3	600.3	123,343			Sine	Medium
EME	3315-3S	4,223	24.2	760.5	32,360			Sine	High
EME	3315-4S	4,390	24.2	760.4	28,620			Sine	High
EME	3329-2S	4,960	22.8	760.4	21,878			Sine	High
EME	3329-3S	4,948	22.6	760.4	27,862			Sine	High
EME	3329-4S	4,897	22.8	760.4	22,734			Sine	High
EME	3339-1S	4,197	22.4	760.4	28,293			Sine	High

```
USE ALL.
COMPUTE filter_$=(Mix = 1).
VARIABLE LABELS filter_$ 'Mix = 1 (FILTER)'.
VALUE LABELS filter_$ 0 'Not Selected' 1 'Selected'.
FORMATS filter_$ (f1.0).
FILTER BY filter_$.
EXECUTE.
UNIANOVA L.Nf50 BY Mode Strain
  /METHOD=SSTYPE(3)
  /INTERCEPT=INCLUDE
  /PLOT=PROFILE(Strain*Mode)
  /CRITERIA=ALPHA(0.05)
  /DESIGN=Mode Strain Mode*Strain.
```

Mix 1. RHMA-G

Univariate Analysis of Variance

Between-Subjects Factors

		Value Label	N
Test Mode	HaverSine		6
	Sine		6
Strain Level	1	Low	6
	2	Medium	6

Tests of Between-Subjects Effects

Dependent Variable: log(Nf-50%)

Source	Type III Sum of Squares	df	Mean Square	F	Sig.
Corrected Model	1.050[a]	3	.350	5.922	.020
Intercept	393.995	1	393.995	6667.519	.000
Mode	.002	1	.002	.036	.854
Strain	1.009	1	1.009	17.079	.003
Mode * Strain	.039	1	.039	.652	.443
Error	.473	8	.059		
Total	395.517	12			
Corrected Total	1.523	11			

a. R Squared = .690 (Adjusted R Squared = .573)

Page 1

Profile Plots

Estimated Marginal Means of log(Nf-50%)
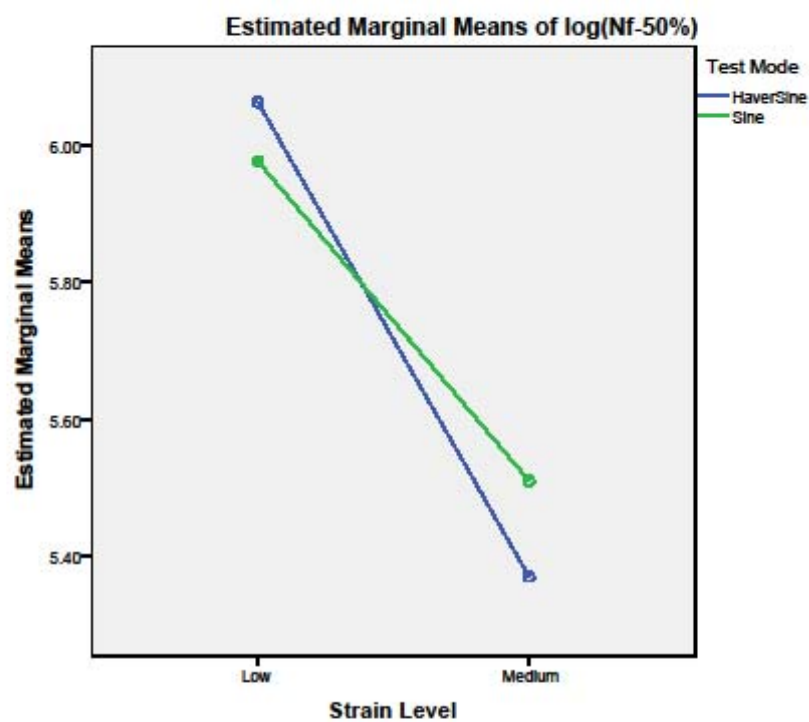
USE ALL.
COMPUTE filter_$=(Mix = 2).
VARIABLE LABELS filter_$ 'Mix = 2 (FILTER)'.
VALUE LABELS filter_$ 0 'Not Selected' 1 'Selected'.
FORMATS filter_$ (f1.0).
FILTER BY filter_$.
EXECUTE.
UNIANOVA L.Nf50 BY Mode Strain
  /METHOD=SSTYPE(3)
  /INTERCEPT=INCLUDE
  /PLOT=PROFILE(Strain*Mode)
  /CRITERIA=ALPHA(0.05)
  /DESIGN=Mode Strain Mode*Strain.

Mix 2. HMA

Univariate Analysis of Variance

Between-Subjects Factors

		Value Label	N
Test Mode	HaverSine		6
	Sine		6
Strain Level	1	Low	6
	2	Medium	6

Tests of Between-Subjects Effects

Dependent Variable: log(Nf-50%)

Source	Type III Sum of Squares	df	Mean Square	F	Sig.
Corrected Model	.385[a]	3	.128	4.223	.046
Intercept	378.900	1	378.900	12477.511	.000
Mode	.103	1	.103	3.381	.103
Strain	.279	1	.279	9.190	.016
Mode * Strain	.003	1	.003	.099	.761
Error	.243	8	.030		
Total	379.528	12			
Corrected Total	.628	11			

a. R Squared = .613 (Adjusted R Squared = .468)

Profile Plots

Estimated Marginal Means of log(Nf-50%)
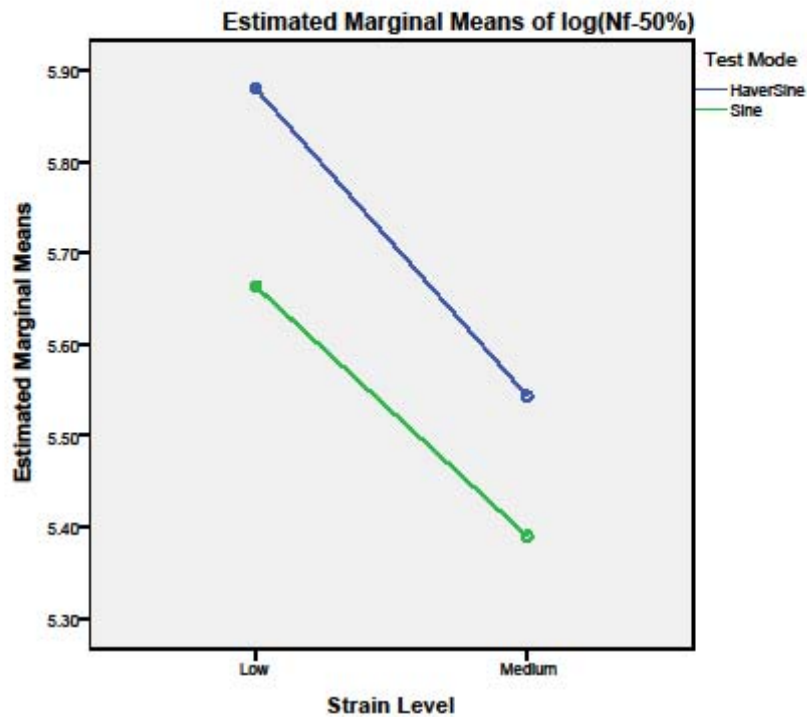
```
USE ALL.
COMPUTE filter_$=(Mix = 3).
VARIABLE LABELS filter_$ 'Mix = 3 (FILTER)'.
VALUE LABELS filter_$ 0 'Not Selected' 1 'Selected'.
FORMATS filter_$ (f1.0).
FILTER BY filter_$.
EXECUTE.
UNIANOVA L.Nf50 BY Mode Strain
  /METHOD=SSTYPE(3)
  /INTERCEPT=INCLUDE
  /PLOT=PROFILE(Strain*Mode)
  /CRITERIA=ALPHA(0.05)
  /DESIGN=Mode Strain Mode*Strain.
```

Mix 3. HMA-PM

Page 4

UCPRC-TM-2015-03

Univariate Analysis of Variance

Between-Subjects Factors

		Value Label	N
Test Mode	HaverSine		6
	Sine		6
Strain Level	1	Low	6
	2	Medium	6

Tests of Between-Subjects Effects

Dependent Variable: log(Nf-50%)

Source	Type III Sum of Squares	df	Mean Square	F	Sig.
Corrected Model	.208[a]	3	.069	.439	.732
Intercept	346.795	1	346.795	2193.401	.000
Mode	.002	1	.002	.015	.905
Strain	.205	1	.205	1.299	.287
Mode * Strain	.000	1	.000	.001	.972
Error	1.265	8	.158		
Total	348.268	12			
Corrected Total	1.473	11			

a. R Squared = .141 (Adjusted R Squared = -.181)

Profile Plots

Estimated Marginal Means of log(Nf-50%)
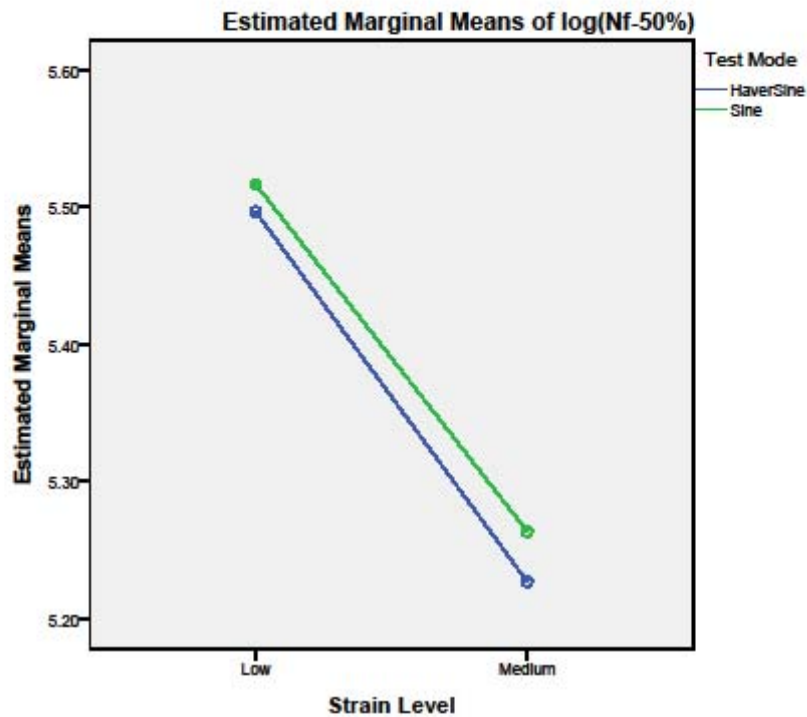

```
USE ALL.
COMPUTE filter_$=(Mix = 4).
VARIABLE LABELS filter_$ 'Mix = 4 (FILTER)'.
VALUE LABELS filter_$ 0 'Not Selected' 1 'Selected'.
FORMATS filter_$ (f1.0).
FILTER BY filter_$.
EXECUTE.
UNIANOVA L.Nf50 BY Mode Strain
  /METHOD=SSTYPE(3)
  /INTERCEPT=INCLUDE
  /PLOT=PROFILE(Strain*Mode)
  /CRITERIA=ALPHA(0.05)
  /DESIGN=Mode Strain Mode*Strain.
```

Mix 4. HMA-RB

Univariate Analysis of Variance

Between-Subjects Factors

		Value Label	N
Test Mode	HaverSine		6
	Sine		6
Strain Level	1	Low	6
	2	Medium	6

Tests of Between-Subjects Effects

Dependent Variable: log(Nf-50%)

Source	Type III Sum of Squares	df	Mean Square	F	Sig.
Corrected Model	.463[a]	3	.154	19.317	.001
Intercept	368.743	1	368.743	46140.880	.000
Mode	.000	1	.000	.038	.851
Strain	.456	1	.456	57.097	.000
Mode * Strain	.007	1	.007	.818	.392
Error	.064	8	.008		
Total	369.270	12			
Corrected Total	.527	11			

a. R Squared = .879 (Adjusted R Squared = .833)

Profile Plots

Estimated Marginal Means of log(Nf-50%)
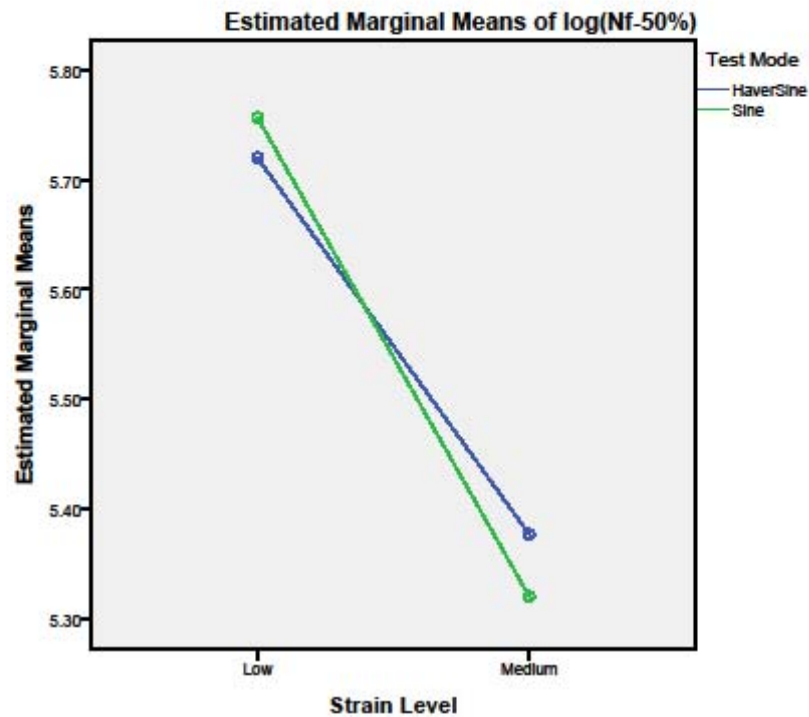
```
USE ALL.
COMPUTE filter_$=(Mix = 5).
VARIABLE LABELS filter_$ 'Mix = 5 (FILTER)'.
VALUE LABELS filter_$ 0 'Not Selected' 1 'Selected'.
FORMATS filter_$ (f1.0).
FILTER BY filter_$.
EXECUTE.
UNIANOVA L.Nf50 BY Mode Strain
  /METHOD=SSTYPE(3)
  /INTERCEPT=INCLUDE
  /PLOT=PROFILE(Strain*Mode)
  /CRITERIA=ALPHA(0.05)
  /DESIGN=Mode Strain Mode*Strain.
```

Mix 5. DC10C320

Page 8

Univariate Analysis of Variance

Between-Subjects Factors

		Value Label	N
Test Mode	HaverSine		8
	Sine		9
Strain Level	1	Low	5
	2	Medium	6
	3	High	6

Tests of Between-Subjects Effects

Dependent Variable: log(Nf-50%)

Source	Type III Sum of Squares	df	Mean Square	F	Sig.
Corrected Model	20.231[a]	5	4.046	563.521	.000
Intercept	445.114	1	445.114	61990.936	.000
Mode	.001	1	.001	.112	.745
Strain	19.736	2	9.868	1374.300	.000
Mode * Strain	.006	2	.003	.452	.648
Error	.079	11	.007		
Total	461.665	17			
Corrected Total	20.310	16			

a. R Squared = .996 (Adjusted R Squared = .994)

Profile Plots

Estimated Marginal Means of log(Nf-50%)
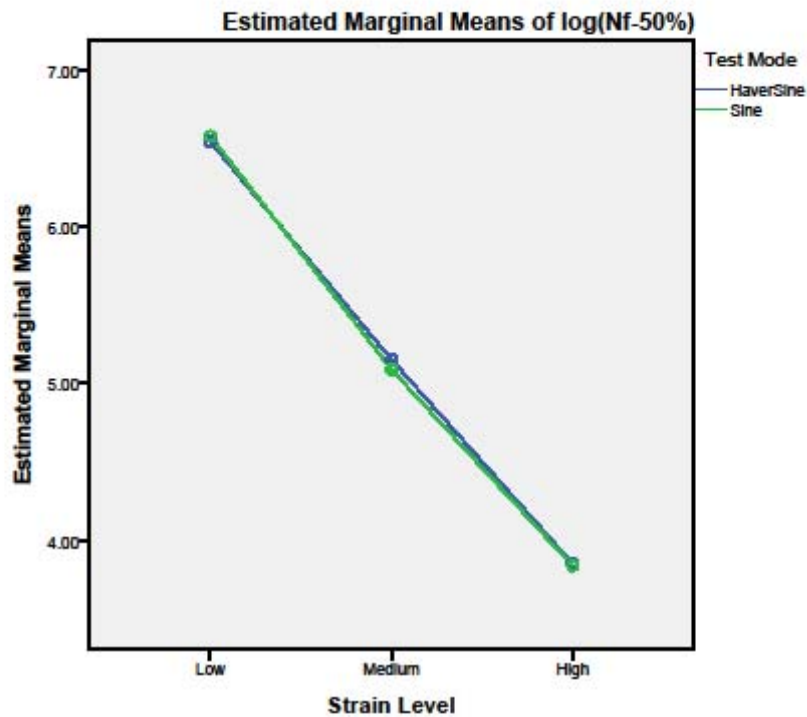

```
USE ALL.
COMPUTE filter_$=(Mix = 6).
VARIABLE LABELS filter_$ 'Mix = 6 (FILTER)'.
VALUE LABELS filter_$ 0 'Not Selected' 1 'Selected'.
FORMATS filter_$ (f1.0).
FILTER BY filter_$.
EXECUTE.
UNIANOVA L.Nf50 BY Mode Strain
  /METHOD=SSTYPE(3)
  /INTERCEPT=INCLUDE
  /PLOT=PROFILE(Strain*Mode)
  /CRITERIA=ALPHA(0.05)
  /DESIGN=Mode Strain Mode*Strain.
```

Mix 6. DC20C600

Univariate Analysis of Variance

Between-Subjects Factors

		Value Label	N
Test Mode	HaverSine		10
	Sine		9
Strain Level	1	Low	7
	2	Medium	6
	3	High	6

Tests of Between-Subjects Effects

Dependent Variable: log(Nf-50%)

Source	Type III Sum of Squares	df	Mean Square	F	Sig.
Corrected Model	10.343[a]	5	2.069	65.023	.000
Intercept	463.584	1	463.584	14572.250	.000
Mode	.898	1	.898	28.216	.000
Strain	9.675	2	4.837	152.059	.000
Mode * Strain	.016	2	.008	.247	.784
Error	.414	13	.032		
Total	487.458	19			
Corrected Total	10.756	18			

a. R Squared = .962 (Adjusted R Squared = .947)

Profile Plots

Estimated Marginal Means of log(Nf-50%)
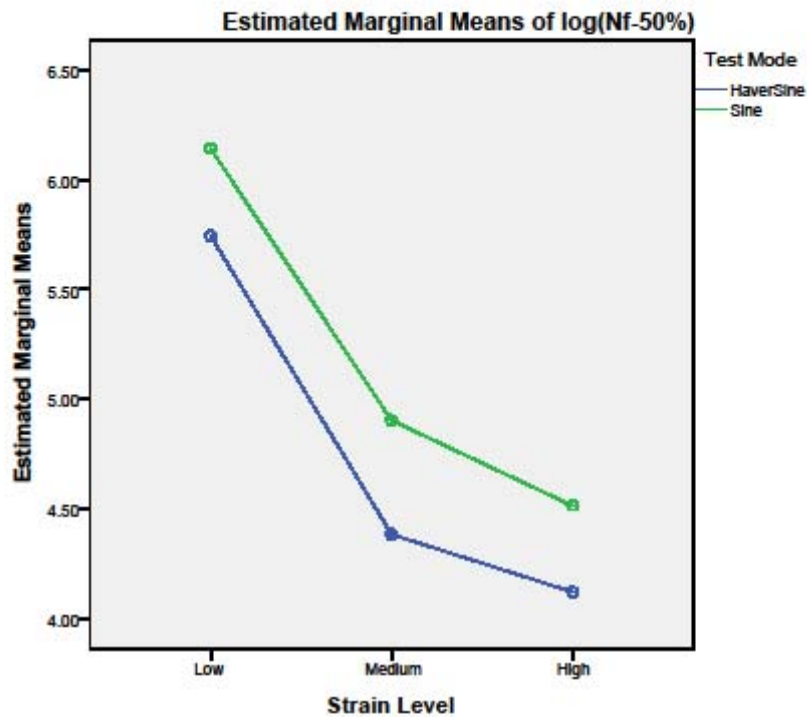
```
USE ALL.
COMPUTE filter_$=(Mix = 7).
VARIABLE LABELS filter_$ 'Mix = 7 (FILTER)'.
VALUE LABELS filter_$ 0 'Not Selected' 1 'Selected'.
FORMATS filter_$ (f1.0).
FILTER BY filter_$.
EXECUTE.
UNIANOVA L.Nf50 BY Mode Strain
  /METHOD=SSTYPE(3)
  /INTERCEPT=INCLUDE
  /PLOT=PROFILE(Strain*Mode)
  /CRITERIA=ALPHA(0.05)
  /DESIGN=Mode Strain Mode*Strain.
```

Mix 7. EME

Page 12

     UCPRC-TM-2015-03

Univariate Analysis of Variance

Between-Subjects Factors

		Value Label	N
Test Mode	HaverSine		10
	Sine		20
Strain Level	1	Low	11
	2	Medium	10
	3	High	9

Tests of Between-Subjects Effects

Dependent Variable: log(Nf-50%)

Source	Type III Sum of Squares	df	Mean Square	F	Sig.
Corrected Model	14.160[a]	5	2.832	101.028	.000
Intercept	698.214	1	698.214	24908.573	.000
Mode	.101	1	.101	3.608	.070
Strain	10.750	2	5.375	191.749	.000
Mode * Strain	.091	2	.046	1.629	.217
Error	.673	24	.028		
Total	839.923	30			
Corrected Total	14.832	29			

a. R Squared = .955 (Adjusted R Squared = .945)

Profile Plots

Estimated Marginal Means of log(Nf-50%)